The atmospheric circulation and dust activity in different orbital epochs on Mars

The atmospheric circulation and dust activity in different orbital epochs on Mars

Claire E. Newman,[a,b,*] Stephen R. Lewis,[a] and Peter L. Read[a]

[a]Atmospheric, Oceanic and Planetary Physics, Department of Physics, University of Oxford,

[*]Corresponding Author E-mail address: claire@gps.caltech.edu

Clarendon Laboratory, Parks Road, Oxford, OX1 3PU, United Kingdom

[b]Division of Geological and Planetary Sciences, California Institute of Technology, Pasadena, CA 91125, USA

ABSTRACT

A general circulation model is used to evaluate changes to the circulation and dust transport in the Martian atmosphere for a range of past orbital conditions. A dust transport scheme, including parameterized dust lifting, is incorporated within the model to enable passive or radiatively active dust transport. The focus is on changes which relate to surface features, as these may potentially be verified by observations.

Obliquity variations have the largest impact, as they affect the latitudinal distribution of solar heating. At low obliquities permanent CO_2 ice caps form at both poles, lowering mean surface pressures. At higher obliquities, solar insolation peaks at higher summer latitudes near solstice, producing a stronger, broader meridional circulation and a larger seasonal CO_2 ice cap in winter. Near-surface winds associated with the main meridional circulation intensify and extend polewards, with changes in cap edge position also affecting the flow. Hence the model predicts significant changes in surface wind directions as well as magnitudes. Dust lifting by wind stress increases with obliquity as the meridional circulation and associated near-surface winds strengthen. If active dust transport is used, then lifting rates increase further in response to the larger atmospheric dust opacities (hence circulation) produced. Dust lifting by dust devils increases more gradually with obliquity, having a weaker link to the meridional circulation.

The primary effect of varying eccentricity is to change the impact of varying the areocentric longitude of perihelion, l, which determines when the solar forcing is strongest. The atmospheric circulation is stronger when l aligns with solstice rather than equinox, and there is also a bias from the Martian topography, resulting in the strongest circulations when perihelion is at northern winter solstice.

Net dust accumulation depends on both lifting and deposition. Dust which has been well mixed within the atmosphere is deposited preferentially over high topography. For wind stress lifting, the combination produces peak net removal within western boundary currents and southern mid-latitude bands, and net accumulation concentrated in Arabia and Tharsis. In active dust transport experiments, dust is also scoured from northern mid-latitudes during winter, further confining peak accumulation to equatorial regions. As obliquity increases, polar accumulation rates increase for wind stress lifting and are largest for high eccentricities when perihelion occurs during northern winter. For dust devil lifting, polar accumulation rates increase (though less rapidly) with obliquity above o=25°, but increase with decreasing obliquity below this, thus polar dust accumulation at low obliquities may be increasingly due to dust lifted by dust devils. For all cases discussed, the pole receiving most dust shifts from north to south as obliquity is increased.

Key Words: Mars, atmosphere; Mars, climate.

1 Introduction

1.1 Motivation

The current state of the Martian atmosphere has provided a challenge to atmospheric modelers, largely because of the importance of atmospheric dust in determining weather and climate. At certain times of year the dust loading and distribution varies greatly from day to day and between years, producing an atmospheric state which, being strongly dependent on this distribution, is also highly variable. The aim is to produce a model which captures a statistically reasonable population of dust storms (as for the Earth, predicting weather phenomena exactly is dependent on the quality of the initial conditions used) and the correct amount of interannual variability. Although progress has been made in using models to study the evolution of dust storms (e.g. Murphy et al. 1995) and in simulating realistic dust storms and cycles with some spontaneous variability (Newman et al. 2002a, 2002b; Basu et al. 2004), many aspects are still uncertain, for example the dust particle size distributions, major source regions and storm decay mechanisms.

Given these difficulties in simulating the current Martian climate, simulating the past climate (with no direct observations and thus apparently fewer constraints on the models) may appear an impossible task. A useful approach is to direct the modeling effort towards understanding some of the observed surface features which change over long time scales. Certain surface features of aeolian origin (produced by the wind), for example, indicate a preferred wind direction other than that currently found, suggesting they were formed during an epoch when dominant wind directions differed (see e.g. Greeley et al. 2002). This suggests using a model to determine which orbital parameters or other factors might have produced such a difference. Regions are observed on Mars which appear to consist of long term dust deposits (e.g. Mellon et al. 2000; Ruff and Christensen 2002), and the ages and thicknesses of these deposits have been estimated (e.g. Christensen 1986). Here the model may be used to estimate both when these regions would last have been eroded, and to predict net accumulation rates for different epochs.

Of particular interest are the polar layered terrains (PLTs), 10-50 m thick layers of dust and water ice which exist polewards of $\sim 80^{\circ}$. In the north the PLT is 4-5 km deep and mostly covered by the residual cap; in the south the PLT is 1-2 km deep and the residual cap, which is off center, covers little – the layered terrain also extends to $\sim 73^{\circ}$S in one quadrant around $\sim 180^{\circ}$longitude. The organization of the layers has been related to orbital variations of Mars (Toon et al. 1980; Pollack and Toon 1982; Laskar et al. 2002), which would have affected atmospheric heating, transport, dustiness and humidity, and hence the relative

rates of water ice and dust deposition and erosion in the polar regions. A full explanation of the PLT's formation requires more complex models which, for example, transport both dust and water, and model the nucleation of water ice onto dust which will clearly affect deposition rates. The polar accumulation rates in the absence of water shown here are, however, a necessary first step.

1.2 Orbital changes over the past few million years

Mars currently has a quite eccentric orbit (eccentricity $e = (a - p)/(a + p)$ =0.0934, where a is the aphelion distance and p the perihelion distance between Mars and the Sun), meaning that at perihelion Mars receives roughly a third more solar insolation than at aphelion. Mars has a planetary obliquity o (angle between the spin axis of the planet and the normal to the orbit plane) of 25.19°, similar to that of the Earth (23.5°). Perihelion occurs at an areocentric longitude (L_s) corresponding to late northern fall – the areocentric longitude of perihelion, l, is 251° (with northern spring equinox, summer solstice, fall equinox and winter solstice occurring at L_s= 0°, 90°, 180° and 270° respectively). Over tens of thousands of years these parameters vary, due to perturbations by other bodies in the solar system and the precession and obliquity variations of Mars's spin axis (Ward 1992; Touma and Wisdom 1993).

Recent work carried out to estimate past variations is expected to be accurate back to roughly 10 Myrs in the past, beyond which point chaotic behavior in the solution becomes significant (Laskar et al. 2002), and may be summarised as follows. The largest variations in e are due to a large amplitude modulating envelope with a period of 2.4 Myrs. The large amplitude variations are as much as 0.115 (from e ∼0 to e ∼0.115), with smaller, higher frequency (95,000–99,000 yrs) changes typically one third as large. The main period in o is about 120,000 yrs, modulated on an ∼1Myr timescale. Over about the past 4 Myrs o has varied between ∼15° and 35°, though from ∼5–10Myrs ago o varied between ∼25° and 45°. Finally, l precesses with a period of about 50,000 yrs.

1.3 The experiments

The experiments are summarized in table 1. The first experiments presented here (o15PAS, presPAS, o35PAS and o45PAS, section 3) simulate the changes in atmospheric circulation and dust transport produced in a Mars general circulation model (MGCM, see section 2) when obliquity is varied from 15° to 45° in steps of 10°. Here dust transport includes atmospheric advection by model winds, atmospheric mixing by vertical diffusion and convective adjustment, gravitational sedimentation of dust through the atmosphere,

Table 1: The experiments and parameter values used

Name	Obliquity o (in °)	Eccentricity e	Longitude of perihelion l (in °)	Passive or active dust	$\alpha_{\rm N}$ (m^{-1})	$\alpha_{\rm D}$ (kg J^{-1})
o15PAS	15	current	current	passive	1.3×10^{-5}	1.6×10^{-9}
presPAS	current	current	current	passive	1.3×10^{-5}	1.6×10^{-9}
o35PAS	35	current	current	passive	1.3×10^{-5}	1.6×10^{-9}
o45PAS	45	current	current	passive	1.3×10^{-5}	1.6×10^{-9}
presAC	current	current	current	active	2.25×10^{-6}	–
o35AC	35	current	current	active	2.25×10^{-6}	–
e0PAS	current	0	current	passive	1.3×10^{-5}	1.6×10^{-9}
l71PAS	current	current	71	passive	1.3×10^{-5}	1.6×10^{-9}
l180PAS	current	current	180	passive	1.3×10^{-5}	1.6×10^{-9}

and injection from the surface via a near-surface wind stress or dust devil lifting parameterization. The dust distribution predicted by the dust transport scheme has no impact on the atmospheric state in these passive runs, but the lifting parameter ($\alpha_{\rm N}$ or $\alpha_{\rm D}$, see section 2.1) for current orbital conditions is still chosen to provide a reasonable match between simulated and currently observed typical dust opacities. This is necessary to estimate the rate of accumulation of surface dust, which also depends on atmospheric transport and dust deposition. For consistency, the same lifting parameter is then used for all passive dust simulations, regardless of the orbital configuration. As discussed above, atmospheric dustiness plays a large part in determining the model state, but for these initial experiments a prescribed dust distribution is presented to the MGCM's radiative transfer routine which has a simple spatial variation and is constant in time (in terms of dust mixing ratios, see section 2.1). This will of course produce strictly inaccurate results, as the total dust load and its spatial distribution actually vary through the year on Mars itself. A variable dust distribution could be prescribed for the current epoch, based on observations, but this would also bias results if used without alteration for other orbital settings.

This problem motivated the running of two active simulations for which the dust distributions are produced by the simulations themselves, using the wind stress dust lifting parameterization only and radiatively active dust transport (presAC and o35AC, section 4). This allows feedbacks between the circulation, dust transport within the atmosphere and dust lifting from the surface. The dust lifting parameterization is tuned to provide a reasonable match to currently observed Mars years without large dust storms for o=25°, and again for consistency is then applied without change to o=35°.

In section 5 the effects of changing eccentricity and time of perihelion are also considered for the present obliquity. First the eccentricity is set to the minimum value possible, e=0, giving a circular orbit which results

in the same total insolation being incident on Mars throughout the year (e0PAS). Two further experiments examine the impact of perihelion occurring shortly before summer solstice in the northern rather than the southern hemisphere (l=71°, l71PAS), and occurring at northern fall equinox (l=180°, l180PAS), for the current eccentricity. Biases towards a stronger circulation during northern winter in each of these experiments are also investigated and discussed.

2 The model and dust lifting parameterizations

2.1 Description

The model used for this work is the Oxford version of the Mars general circulation model developed jointly at the sub-department of Atmospheric, Oceanic and Planetary Physics at the University of Oxford and the Laboratoire de Météorologie Dynamique du Centre National de la Recherche Scientifique in Paris. The model used here (the MGCM) is almost identical to the Oxford version described in Forget et al. (1999), though with some changes including a different formulation of the radiative transfer code. Unless otherwise specified it is run at relatively low horizontal resolution (spectral truncation T21, with dust stored on a 7.5° × 7.5° grid). The vertical resolution used is as in Lewis et al. (1999), with the lowest level at ∼5m, levels closely spaced through the boundary layer, and 25 levels in all up to ∼90km. The MGCM used here also includes the dust transport scheme described in Newman et al. (2002a, 2002b), though with near-surface wind stresses now calculated after the vertical diffusion scheme is applied to the model wind field, giving generally lower values; it does not include transport of water vapor and water ice particles.

In the experiments shown here the dust transport scheme was run using a single dust particle size of 1μm radius, with dust as either a passive or an active tracer. In the latter case the MGCM's radiation code sees the changes to the atmospheric dust distribution which are simulated by the scheme, and responds accordingly, using radiative dust properties representative of the observed size distribution (rather than 1μm particles). In the former case the radiation code sees a prescribed dust distribution, and in the passive dust experiments shown here a moderate background level of dust loading is used. Visible dust opacity referenced to the 700Pa pressure surface is 0.2 at all times and locations, with the vertical distribution given by

$$q = q_0 \exp\left\{0.007\left[1 - (p_0/p)^{(70\mathrm{km}/\mathrm{z_{max}})}\right]\right\}, \quad (1)$$

where q=mass mixing ratio, q_0=a reference value which results in the required dust opacity (0.2 at 700Pa

here), p and p_0 are pressure and reference pressure (700Pa here) respectively, and $z_{\max}$=30km (this is low for times of strong dust activity, but probably higher than during the clearest periods). As shown in Fig. 3 of Lewis et al. (1999), this produces a sharp exponential decline in dustiness to the dust top height of $z_{\max}$.

The lifting parameterizations used are similar to some of those described in Newman et al. (2002a). Lifting by near-surface wind stress ζ is modeled using a slightly simpler method than in Newman et al. (2002a), which required three parameters to be specified and calculated threshold wind stresses at each gridpoint and time. Here dust is lifted when a constant threshold wind stress ζ^{t} is exceeded (here 0.01N/m^2), with the lifted dust flux given by

$$\alpha_{\mathrm{N}} \times 2.61 \frac{\zeta^{3/2}}{g\sqrt{\rho}} \left(1 - \sqrt{\frac{\zeta^{\mathrm{t}}}{\zeta}}\right) \left(1 + \sqrt{\frac{\zeta^{\mathrm{t}}}{\zeta}}\right)^2, \tag{2}$$

where g=gravitational acceleration and ρ=near-surface atmospheric density. Thus only two parameters are involved (ζ^{t}, and α_{N} which determines the actual amounts lifted). Although the same threshold stress is used in all experiments shown in table 1, it would be unphysical to apply the same value of α_{N} to both passive and active dust simulations. The active dust runs (which include the impact of dust on the Martian climate, hence are more realistic) allow strong positive feedbacks between dust loading, circulation strength and further lifting, and therefore produce far higher peak opacities than produced by passive simulations for the same value of α_{N} (Newman et al. 2002b). The value of α_{N} is therefore chosen to be 1.3×10^{-5} m^{-1} for all passive dust simulations, and 2.25×10^{-6} m^{-1} (almost 6 times smaller) for all active dust simulations. In both cases it is chosen to produce peak zonally averaged, visible atmospheric dust opacities of $\sim$1 in northern low latitudes for the two simulations run using present day orbital settings (presPAS and presAC), in line with peak visible opacities observed or inferred for a typical Mars year (Clancy et al. 2000; Smith et al. 2001; Liu et al. 2003; Smith 2004).

Lifting by dust devils is set proportional to the 'dust devil activity', with constant of proportionality α_{D}. The dust devil activity is a measure of how much energy is available to drive the dust devils, defined by Rennó et al. (1998) as roughly the thermodynamic efficiency of the dust devil convective heat engine multiplied by the surface sensible heat flux. The former increases with convective boundary layer height, while the latter is the heat input to the base of the dust devil, which is positive if the surface temperature exceeds that of the atmosphere above it. Lifting by dust devils may be ubiquitous (e.g. Edgett and Malin 2000) and may contribute to a large fraction of the dust lifted (Ferri et al. 2003; Basu et al. 2004), except during the storm season when wind stress lifting probably dominates in producing any large dust storm

events (Cantor et al. 2001; Newman et al. 2002b; Basu et al. 2004). Using a value of $\alpha_{\rm D}$=1.6$\times$10^{-9} kg J^{-1}, which produces peak opacities of $\sim$1 during the storm season for the present orbital settings, may therefore overestimate the amount of dust devil lifting at this time of year in particular, but is used to calculate dust devil lifting in the passive dust experiments for comparison with the wind stress lifting results. Experiments with both lifting mechanisms and active dust transport are an obvious next step, following on from the active dust simulations with wind stress lifting shown in section 4, but were not included in this initial work as they greatly increase the sensitivity of results to the parameters chosen and hence the complexity of analysis.

2.2 Performance of the lifting parameterizations for current orbital settings

2.2.1 Comparison with observations

It is important to assess the performance of the dust lifting parameterizations for the present epoch before proceeding. Wind stress lifting is thought to be dominant in producing dust storms, thus predicted wind stress lifting sites can be compared with observed initiation regions of large dust storms observed between L_s=120° and L_s=270° during the first year of Mars Global Surveyor (MGS) observations. Figure 1 shows plots of the annual thickness of dust lifted for five shorter periods, then for the entire longer period, as predicted by a present day simulation which used radiatively active dust transport with wind stress lifting only (experiment presAC). The lifted dust flux (from equation 2) is converted to dust thickness by assuming a dust density of 2500kg m^{-3}. Superimposed on this are asterisks marking storm initiation sites extracted from Mars Orbiter Camera (MOC) images (Cantor et al. 2001). Haberle et al. (2003) performed a similar comparison between lifting predicted by the NASA Ames Mars general circulation model and MOC storm observations. They defined 'deflation potential' as the thickness of dust which would be removed over a given period of time (typically 1 year), but used a simpler formula to calculate the lifted dust flux. They also used a larger threshold stress than used in the MGCM (0.02Nm^{-2}), which reflects the fact that MGCM surface winds are generally slightly lower in magnitude than those produced by the model of Haberle et al. (2003).

Looking at the final plot for the entire period, there are regions of good agreement between MGCM predictions and MOC observations. In particular, the model predicts the lifting observed to the east of the highlands of Tharsis, Syrtis and Elysium. These locations experience enhanced meridional flows known as western boundary currents (WBCs, see e.g. Joshi et al. 1995). The clear regions between these positions in the range $\sim$60°N to 20°S coincide in the model and observations. From L_s=240°–270°, the MGCM predicts

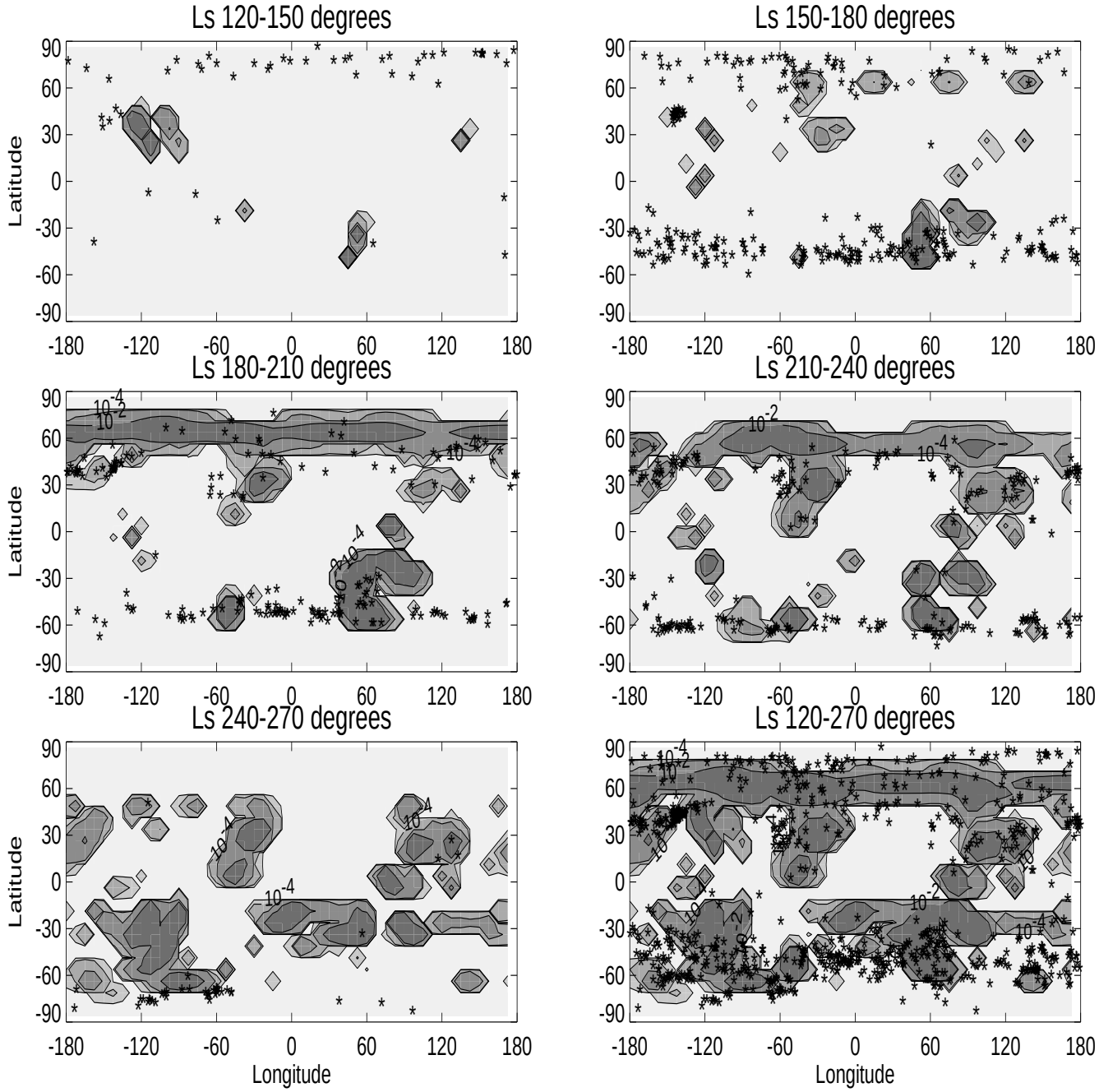

Figure 1: Newman et al. Predicted wind stress lifting and MOC storms observed.

far more lifting than suggested by observations of initial dust clouds, in the region $\sim$25°–35°S where strong north-westerlies associated with the zonal mean circulation are produced. However, elevated dust levels due to regional storms in the period $L_s \sim 230°$–$270°$ may have obscured individual lifting events.

The MGCM captures some (though not all) of the band of lifting in southern spring-summer which moves polewards with time. This movement suggests it is at least partly due to strong near-surface winds near the retreating polar cap edge, a region of strong temperature gradients giving rise to thermal contrast and baroclinic flows, which the MGCM models as retreating at just such a rate. Interestingly, the passive dust simulation (presPAS) does not predict as much lifting within this band, particularly as the band moves to higher latitudes, suggesting that the atmospheric dust distribution (and its effect on surface winds) in the active case is more realistic than in the passive case (where a more uniform prescribed distribution is used in the radiative transfer scheme). The best match between observed and predicted cap edge lifting occurs when strong cap edge flows are combined with slope winds in the Hellas and Argyre basins. The lack of lifting at other longitudes along the receding cap edge may be due to the precise choice of lifting threshold, or the low model resolution may prevent the model from resolving small scale thermal contrast flows, slope winds and/or wave activity. A similar lack of lifting early on in northern polar regions may be due to the MGCM having no water ice cap, hence cap edge flows only become possible when the seasonal CO_2 ice cap begins to form in late fall.

Mapping of dust devil activity observed on Mars is still underway, making it difficult to assess conclusively the performance of the lifting parameterization used here, although it has been shown to be consistent with what observations are currently available (Newman et al. 2002a). A comparison with the observations of initial storm clouds shown in Fig. 1 is probably inappropriate, given that observations show no correlation between dust devils and storm initiation (Cantor et al. 2001), and that simulations which assume dust devils to be the primary lifting mechanism for Mars produce far more lifting (and consequently far higher dust opacities than observed) during northern spring and summer (Newman et al. 2002b). Fig. 7 (discussed in section 3.2.2) includes a plot showing regions of peak dust devil lifting for the current epoch, and as expected these do not match the observations shown in Fig. 1.

2.2.2 Dust lifting rates and the benefits of a dust transport scheme

In terms of patterns of wind stress lifting there is reasonable agreement between the results shown in the final plot of Fig. 1 and those shown in figure 4 of Haberle et al. (2003). There are significant differences,

however, in the amount of lifting predicted. For o=25°, for example, the MGCM predicts just under 0.01cm of dust lifted per year in peak lifting regions, whereas Haberle et al. (2003) find a peak deflation potential greater than 10cm per year. Haberle et al. (2003) do not include dust transport in the version of their model used to calculate deflation potential, but these results suggest that, were they to do so, their higher lifting rates would probably produce orders of magnitude higher (and thus unrealistic) atmospheric dust opacities than produced by the MGCM. This emphasizes the usefulness of including dust transport schemes within Mars models if quantitative estimates of dust lifting rates (hence also deposition and net accumulation rates) are of interest, as this allows the lifting parameter (here α_{N}) to be chosen on the basis of producing realistic atmospheric opacities. Results using the GFDL Mars model (Basu et al. 2004), which also tunes the dust injection to produce realistic opacities, support the smaller deflation potentials predicted by the MGCM.

3 The effect of varying obliquity using passive dust transport

3.1 The atmospheric circulation

This has already been discussed in detail by previous authors (Fenton and Richardson 2001; Haberle et al. 2003; Mischna et al. 2003) so the current section gives only a brief overview of the main results, followed by a description of selected points including the main differences found between this and previous work.

3.1.1 Overview

The basic idea is that changing a planet's obliquity alters the distribution of solar heating across its surface. For Mars, with a primarily CO_2 atmosphere, the major effect is on the formation / removal of CO_2 surface ice. At low obliquities the poles never receive much solar insolation, resulting in a lowering of their annual mean surface temperatures and hence a CO_2 ice build-up. Below some critical obliquity, between 15° and 25° in the MGCM and ∼21.6° in the energy balance model of Fanale and Salvail (1994), permanent CO_2 ice caps therefore exist at both poles. At high obliquities, the polar regions receive far more solar insolation during summer and less during winter, hence the summer pole is free of CO_2 ice but large seasonal CO_2 caps form at the winter pole. This results in an increase in the amplitude of the annual pressure cycle (which for all obliquities has peaks in early northern and southern summer, when the summer seasonal cap has largely sublimed but the winter cap is still midway through forming). Plots of globally averaged surface temperature in the MGCM are similar to those shown in Fig. 5 of Haberle et al. (2003). Plots of

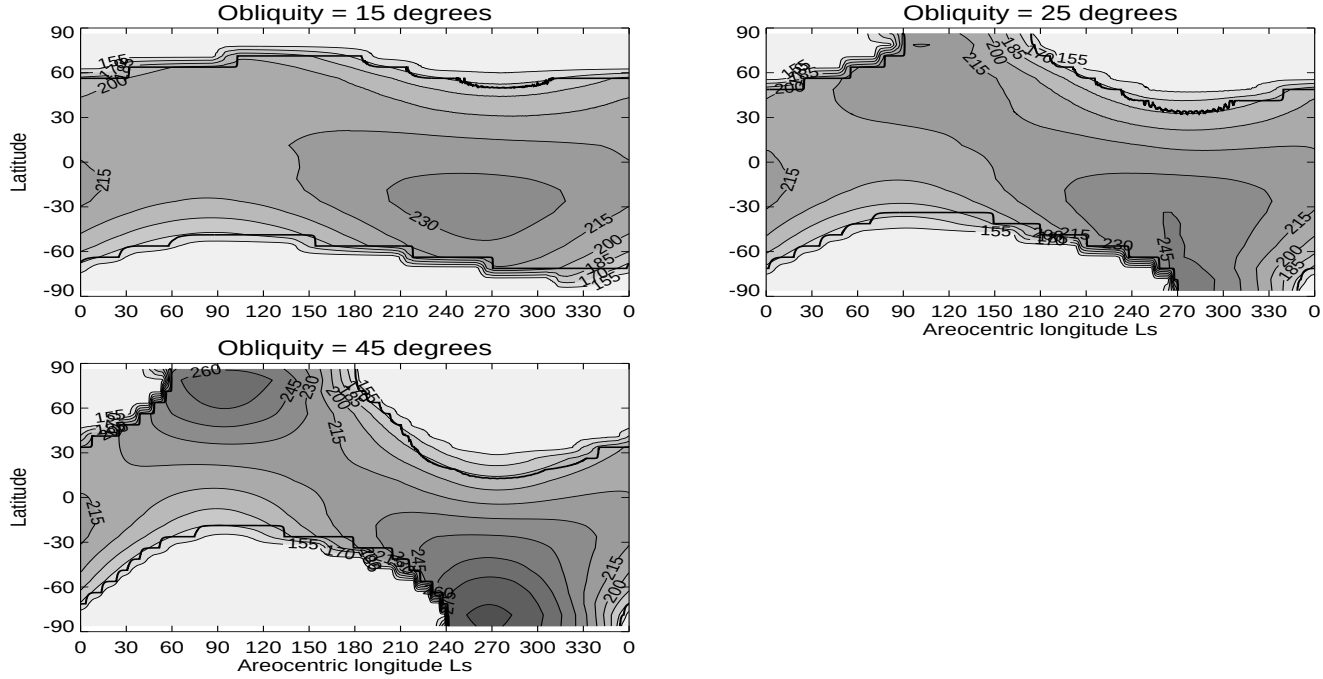

Figure 2: Newman et al. Zonal mean surface temperature and CO_2 ice cap edge.

globally integrated atmospheric mass are very similar to those shown in Fig. 1 (giving results only for o=25° and higher) of Mischna et al. (2003). Equivalent plots of globally averaged surface pressure are very similar to results for o=25° and higher shown in Fig. 8 of Haberle et al. (2003), although differ from the latter for lower obliquities due to the effect on surface pressure of polar ice accumulation in the MGCM (see section 3.1.2).

Figure 2 demonstrates the effect of varying obliquity on surface temperatures and CO_2 ice cover, and is similar to Fig. 6 of Haberle et al. (2003) except that the cap edge is defined here as the latitude at which the zonal mean CO_2 ice cover exceeds 1kg m^{-2} (rather than as the latitude for which one or more grid points has ice cover, as in Haberle et al. (2003), which would tend to make the caps appear larger than shown here). As obliquity increases, peak surface temperatures move to higher summer latitudes, and in the winter hemisphere the seasonal CO_2 cap reaches to lower latitudes (though never reaches the equator, except at a few longitudes for o=45°) thus pinning surface temperatures at the CO_2 frost point ($\sim$150K) over much of the planet. Except for a 'bunching up' of temperature contours at the edge of increasingly large residual caps (and colder surface temperatures at latitudes where the cap is present at one obliquity but not at another), equinoctial surface temperatures vary little with obliquity.

The stepped nature of the zonal mean cap edge position shown in Fig. 2 is due to the fact that entire gridpoints are cleared of / gain ice cover at a time, rather than this happening smoothly and incrementally as

on Mars itself. This also affects the zonal mean surface temperatures (and low level atmospheric temperatures, not shown) at the receding cap edge, where removal of ice from an entire gridpoint allows the surface to warm rapidly from the CO_2 frost point to temperatures representative of ice-free regolith. The reverse effect does not occur during cap formation, as at this time the surrounding atmosphere cools beforehand, buffering the effect. The step sizes are related to the grid resolution used, thus MGCM simulations run at higher resolution show a smoother variation in cap edge surface temperatures. Similar step features occur in plots of global mean surface temperature predicted by the MGCM, and are very nearly identical to those shown in Fig. 5 of Haberle et al. (2003), since both models used comparable horizontal resolution.

Figure 3 shows the effect of increasing obliquity on zonal mean zonal winds and temperatures, and the meridional transport circulation (here given approximately by the residual mean circulation, see e.g. *Andrews et al.* [1987]). The left-hand column shows the current circulation predicted by the MGCM in northern winter using the moderate dust distribution described in section 2.1. Near both solstices a cross-equatorial Hadley circulation dominates, with the position of the rising branch in the summer hemisphere being linked to the latitude of maximum time-integrated solar heating. As obliquity is increased (right-hand column), the subsolar latitude increases, as does the fraction of each latitude circle in the summer hemisphere which receives solar insolation at any given time (though of course this fraction never exceeds one, hence once this is reached no further increase is possible). The net result is that the rising branch shifts to higher latitudes as obliquity increases. Angular momentum constraints allow the entire Hadley cell to broaden, increasing downwelling over the winter pole and hence the amount of polar warming produced and strength of the circumpolar vortex. The meridional circulation also strengthens, with the stronger cross-equatorial flow producing larger easterlies aloft.

At equinox (not shown) there is little difference between results for different obliquities. In both cases the mean meridional circulation consists of two Hadley cells rising near the equator and extending only to $\sim 40^\circ$, with far lower flow velocities than are encountered near solstice.

3.1.2 The impact on mean surface pressure at low obliquities

The removal of atmospheric CO_2 as surface ice results in a reduction of atmospheric pressure, if the total amount of CO_2 present remains constant (as is assumed in the MGCM). The MGCM does not currently consider other CO_2 reservoirs, such as CO_2 in the high latitude regolith (Toon et al. 1980; Pollack and Toon 1982). At current surface pressures a decrease in high-latitude temperatures (at low obliquities) would tend

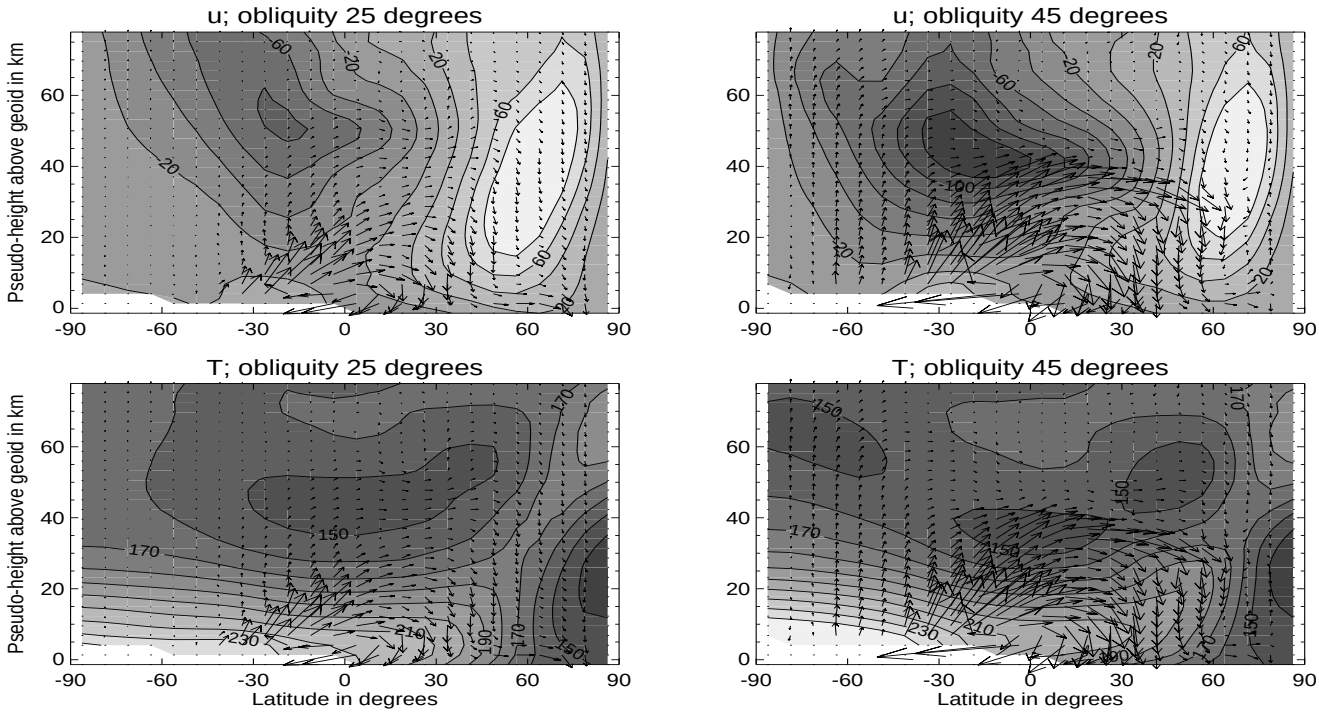

Figure 3: Newman et al. The zonal mean northern winter solstice circulation for o=25°and 45°.

to increase CO_2 adsorption rates, although the reduction in surface pressure due to increased cap deposition would tend to produce the opposite effect and reduce adsorption rates, actually releasing more CO_2 again (Fanale and Salvail 1994). Most of any additional CO_2 released would likely condense onto the caps, however, so surface pressure estimated neglecting the regolith adsorption may be approximately correct, although the amount of ice formed is probably an underestimate.

Figure 4 shows the variation of surface pressure over several years for obliquities 5° and 15°, predicted using the same value of total CO_2 (surface ice plus atmospheric) as was used in all the other simulations (and which produces a realistic mean surface pressure for current orbital parameters). In both cases the MGCM was run until the mean pressure approached some asymptotic value, the permanent CO_2 ice caps having built up year by year. The final value of global mean surface pressure is ∼40Pa after 12 years for o=5° and ∼350Pa after 27 years for o=15°. The surface pressure reached for o=15° is slightly higher than that predicted by Fanale and Salvail (1994), who estimated a surface pressure of ∼ 270Pa for o=15° using a latitude and depth dependent thermal model. These results represent the first time that a full general circulation model has been used to estimate such changes, and also demonstrate that the MGCM is still able to operate usefully for conditions very different to those which exist today. It should be noted that the total column dust opacity prescribed for these low obliquity runs also decreases with surface pressure, because

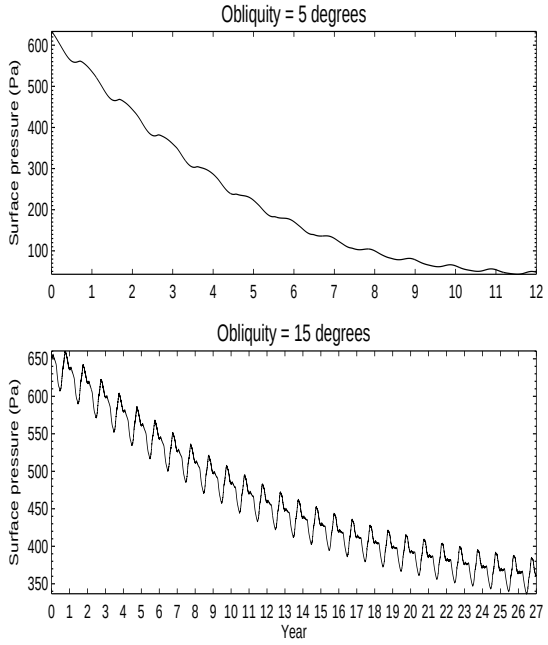

Figure 4: Newman et al. Surface pressure for 5 and 15° obliquity.

the dust is prescribed to have a constant opacity – but at a reference pressure of 700Pa – in all of the passive dust experiments (see section 2.1).

Once no permanent caps exist the model of Fanale and Salvail (1994) predicts that increased summer temperatures, tending to release more CO_2 from the high latitude regolith, are balanced by the effect of the increased surface pressures (causing the regolith to adsorb more CO_2), hence resulting in little variation in mean surface pressure at high obliquities. There may also be increased adsorption into the low latitude regolith. The permanent caps disappear at an obliquity of $\sim$32.3° in their model, by which point a mean surface pressure of $\sim$710Pa (slightly higher than the current value) has been achieved owing to the release of CO_2 from the caps. In the MGCM, by contrast, the annual mean surface pressure is slightly lower at o=35° and 45° than for the current obliquity, due to the huge seasonal caps remaining large further into spring (as shown in Fig. 2 by the more gradual initial retreat as obliquity increases).

3.1.3 Surface wind patterns and aeolian features

The surface wind pattern is key to the formation of many surface features and to dust lifting by near-surface wind stress. Figure 5 shows surface winds averaged over 10 sols at L_s= 90°, 180° and 270° (northern summer, fall and winter respectively) for three obliquities. The cross-equatorial flow at solstice – the return branch of the Hadley circulation, which is concentrated into WBCs as discussed in section 2.2 – becomes

stronger and extends to higher summer latitudes as obliquity is increased and the Hadley circulation becomes stronger and broader. By conservation of angular momentum, as these flows move away from the equator they are turned towards the east, producing increasingly strong summer mid-latitude westerlies extending to increasingly high latitudes. In the winter hemisphere, increasing coverage by the seasonal cap leads to broad areas (those covered by the cap but away from its edge) with low surface temperature gradients, hence limits near-surface wind magnitudes. The location of the cap edge, at which a strong thermal contrast exists, also has a large effect. For example, during fall when local thermal contrast / topographic flows dominate (see e.g. Siili et al. 1999), the cap edge lies across the southern slopes of the Argyre and Hellas basins at low obliquity, hence daytime off-cap winds are in the same direction as nighttime downslope winds over the adjacent regolith (with winds continuously downslope over icy slopes). Yet by o=45° the cap edge lies across the middle of the basins, hence daytime off-cap winds and daytime upslope winds over the adjacent regolith are in the same direction, producing even stronger surface winds further equatorwards than for the lower obliquity. Thus the main differences in dominant surface wind velocities, due to changes in obliquity, are predicted to occur in the mid to high latitude range affected by the change in Hadley cell and cap extent at a particular time of year, and may include changes in direction as well as magnitude.

Fenton and Richardson (2001) concluded that surface wind directions were essentially unchanged by variations in obliquity, but focused on changes associated with the Hadley circulation, and also limited their investigation to a maximum of 35° obliquity. In MGCM results for o=35° (not shown) the expansion of the Hadley cell at the surface is in fact quite small despite a larger expansion aloft, whereas there is significant expansion even at the surface (as shown in Fig. 5) by 45°. This suggests a bias towards the low level Hadley circulation being constrained equatorwards of ∼40°S in the southern summer hemisphere, perhaps due to the Martian topography.

The most direct way to verify these predictions would be to identify aeolian features in the same region of Mars which show evidence of having been produced under different dominant wind regimes. For example at ∼40°N, 40°W, the MGCM predicts strong westerlies or west-south-westerlies at o=45°, peaking during northern summer, whereas for the present day it predicts that the strongest winds are north-easterlies occuring during northern fall and winter. Similar behavior is predicted for ∼40°N, 110°E. Ideal features would be yardangs (streamlined features carved by wind abrasion by dust and sand, typically highest and broadest at the blunt end that faces into the wind), ventifacts (rocks with pits, flutes and facets caused by wind abrasion, many with the alignment of grooves and pits recording the prevailing wind direction) or dunes (whose type

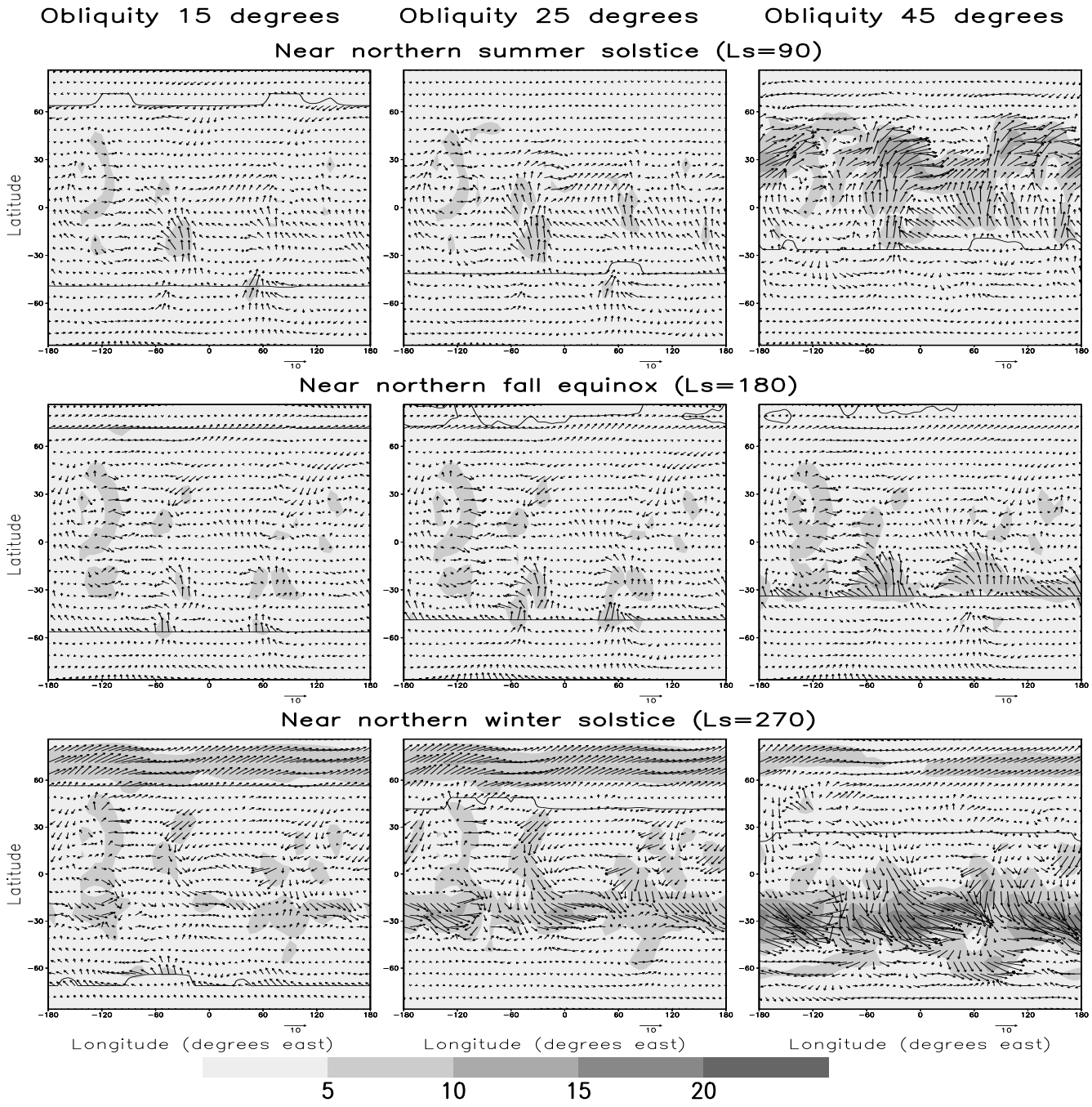

Figure 5: Newman et al. Near-surface winds for three obliquities.

and shape often indicate the dominant wind direction during formation). Wind streaks (due to either the removal or deposition of material, generally bright dust) are less useful as they typically represent only current wind regimes.

Unfortunately, it is difficult to observe ventifacts, yardangs and dunes in sufficient detail. Ventifacts are too small to be observed from orbit, so can only be seen in lander images. Yardangs are larger and hence more visible, but it is still difficult to determine the sense of prevailing winds (rather than just their orientation) without high resolution imaging. Both the direction and sense of prevailing winds can be obtained relatively easily from certain dune types, e.g. barchan dunes, though again this requires sufficiently high resolution imaging of dune fields. Observations targeting aeolian features, specifically yardangs and dunes, in the regions of interest discussed above could be used to validate the MGCM's predictions of changes in surface wind patterns, which would also indirectly validate its predictions of seasonal cap extent and circulation changes for different orbital configurations.

Thus far, the Mars Pathfinder landing site ($\sim$19.3°N, 33.6°W) is the only location on Mars for which there exists strong evidence for a change in wind direction using these techniques. Dominant winds here were inferred to be from the north-east, by observing the orientation of nearby bright features assumed to be dunes imaged from orbit, and the direction and sense of depositional wind streaks and tails in the lee of obstacles seen both from orbit and in Pathfinder images (e.g. Greeley et al. 1999). The MGCM, in agreement with other Mars models (e.g. Fenton and Richardson 2001; Haberle et al. 2003), also currently predicts dominant winds from the north-east in this region (occurring during northern winter). Yet the Pathfinder images also show flutes and ventifacts on rocks which indicate prevailing winds from the east-south-east (e.g. Bridges et al. 1999), raising the possibility that under different orbital conditions this might have been the dominant wind direction (Greeley et al. 2000). Experiments conducted using the MGCM at higher obliquities do indeed show a change in dominant wind direction here by o=45°, due to the presence of increasingly strong southerlies/south-westerlies in northern summer as the strength of the meridional circulation at this time of year increases, whilst northern winter wind magnitudes here drop due to increased ice cover over the northern hemisphere. For sufficiently high dust levels (e.g. as in the active dust transport experiments described in section 4) northerlies/north-easterlies during northern winter may again dominate if the size of the seasonal cap is reduced in a warmer atmosphere. But for none of the cases described here (including varying eccentricity and areocentric longitude of perihelion for the current obliquity, see section 5) does the MGCM predict east-south-easterlies to dominate in this region. This result is in agreement with

the findings of Fenton and Richardson (2001) and Haberle et al. (2003), and suggests a cause other than solely variations in orbital parameters.

3.2 Dust transport

3.2.1 The latitudinal variation of dust lifting and deposition

The upper two rows in Fig. 6 show zonal mean dust lifting by near-surface wind stress (top) and dust devils (bottom) respectively using the simple parameterizations described in section 2.1, for o=25° and 45° (experiments presPAS and o45PAS). The results were produced using passive dust transport, and for wind stress in particular are also dependent on the choice of parameter values, but still provide insight into the variation of dust processes with obliquity. The MGCM currently predicts little interannual variability in dust lifting for all lifting parameters used. For high threshold wind stresses, and using radiatively active dust transport, a small amount is produced in terms of the appearance (or not) of a cross-equatorial dust storm (*Newman et al.* 2002b), but overall there is less interannual variability than observed on Mars itself. The results shown here are therefore taken from a single year-long simulation (following an initial 'spin-up' year), as results are unlikely to differ significantly from averaged results of multi-year simulations.

Near-surface wind magnitudes (see section 3.1.3), wind stress and hence wind stress dust lifting greatly increase overall with obliquity, with the latter two particularly suppressed at o=15° due to the reduced surface pressure. Lifting peaks during northern winter for all obliquities. For high obliquities this is due to the stronger global circulation at this time and the associated strong near-surface winds (peaking in the summer hemisphere), but for low obliquities it is also due to the presence of strong baroclinic and cap edge flows in the winter hemisphere due to strong high latitude temperature gradients in the vicinity of the winter ice cap edge. The latter decrease in relative importance as obliquity increases (as this results in the cap edge shifting to lower latitudes and the mean meridional circulation becoming increasingly dominant). Lifting during northern summer becomes significant for higher obliquities, as the global mean circulation and related surface winds increase in strength, though there is still less lifting than at the opposite solstice. This asymmetry is enhanced in active dust experiments for which positive feedbacks exist between dust amounts and wind stress lifting (see section 4).

For all obliquities, peak dust devil lifting occurs at ∼25° north or south during northern or southern summer respectively, rather than following the sub-solar point (the position of peak instantaneous surface heating) which is shifted polewards with obliquity for any given sol in summer. The reason is that heating of

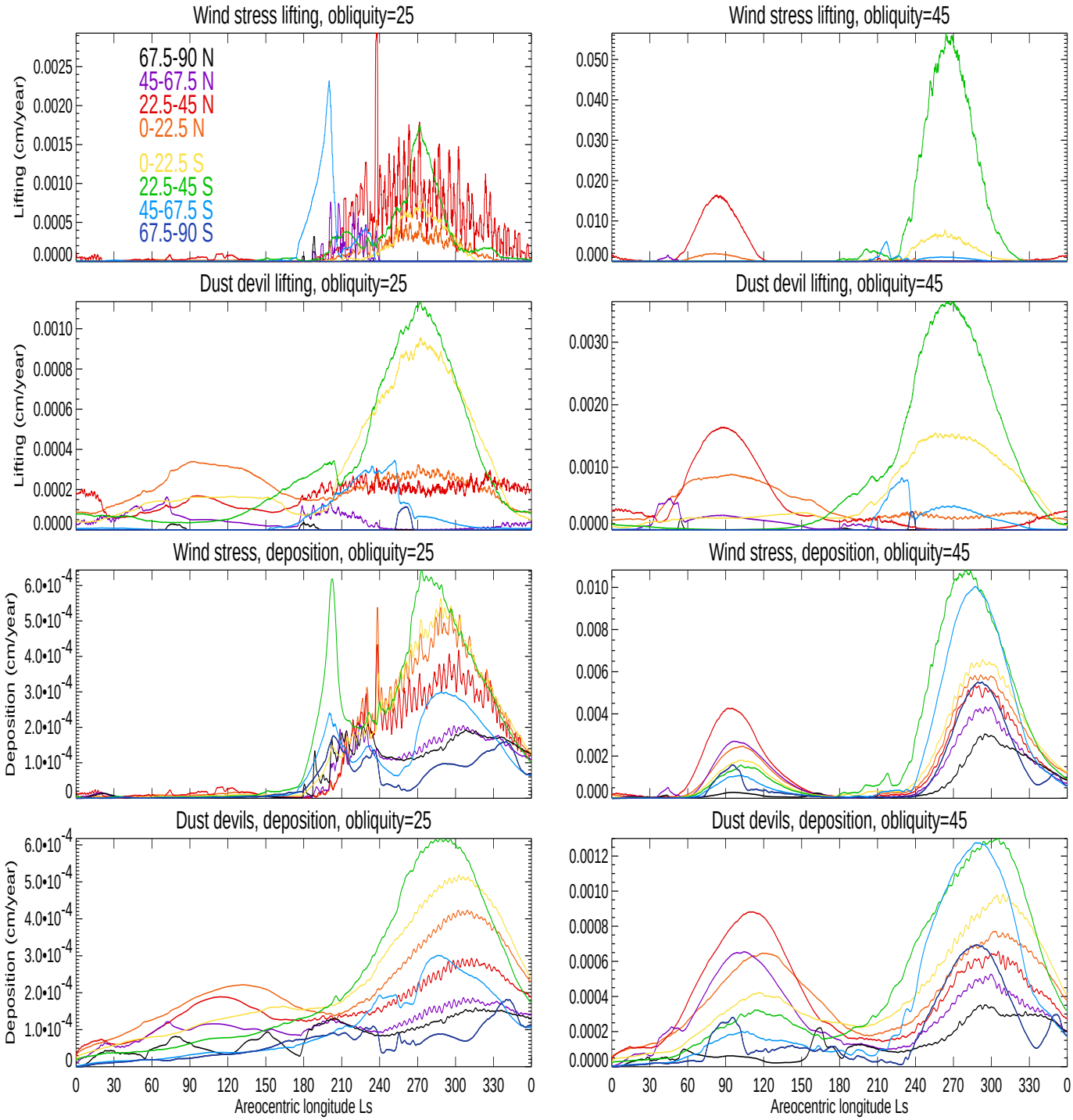

Figure 6: Newman et al. Dust lifting and deposition for two obliquities for wind stress and dust devil lifting.

the lower atmosphere also peaks at increasingly high latitudes. The surface to level 1 (at $\sim$5m) temperature difference in summer in fact peaks at $\sim$25° for all obliquities, the latitude at which there is the strongest day-night temperature difference, hence where atmospheric temperatures lag surface temperatures most strongly. This result may be somewhat model dependent, however, as this lag will be affected by a variety of factors including the particular soil model and boundary layer scheme used. The roughly threefold increase in dust devil lifting within the o=25°– 45°S latitude band (which is far less than the increase found for wind stress lifting) is related to the formation of a thicker convective boundary layer in the peak lifting regions, which increases the predicted thermodynamic efficiency of the dust devil heat engines. There is also a slight dependence on wind stress (via the sensible heat flux calculation).

The lower two rows of Fig. 6 show zonal mean dust deposition for the same experiments. The total amount of dust deposited increases with obliquity, since increased lifting rates result in a dustier atmosphere. As expected, due to atmospheric transport there are differences between patterns of lifting and deposition. For example, using wind stress lifting, deposition at high northern latitudes relative to that elsewhere is about the same for both obliquities shown, despite a huge decrease in the relative amount of northern lifting for o=45°. This reflects strong cross-equatorial transport extending to polar regions (polar accumuation rates are discussed further in section 3.2.4). Yet overall trends are reproduced, e.g. for wind stress lifting both lifting and deposition shift from peaking in northern to peaking in southern latitudes as obliquity is increased.

These passive dust results show wind stress lifting and deposition becoming increasing similar to that predicted for dust devils as obliquity is increased. This is a direct result of the main meridional circulation becoming stronger, and its associated surface winds dominating over those linked to cap edge effects, baroclinic instability, etc.. Thus the main forcing behind wind stress lifting becomes more closely tied to the seasonal variation in solar forcing which strongly controls dust devil lifting. Wind stress lifting still shows more asymmetry than dust devil lifting between the two solsticial seasons, because while dust devil lifting responds more directly to changes in heating rates (and to the increased solar insolation during southern summer), wind stress lifting responds via the impact on the circulation, which is non-linear with respect to insolation changes. The hemispheric dichotomy in topography, which consists of much of the northern hemisphere standing several kilometers lower than the south, with the south pole nearly 6km higher than the north, also produces a fundamental bias towards a stronger meridional circulation in southern summer (see section 5.1). In active dust runs this asymmetry is enhanced for wind stress lifting, which has positive feedbacks on further lifting (Newman et al. 2002a), and reduced for dust devil lifting (which has negative

feedbacks), hence in active runs wind stress and dust devil results do not become similar (in either magnitude or pattern) as obliquity increases.

3.2.2 Patterns of net dust accumulation

Figure 7 shows the thickness of dust lifted (contours) in one year and the net change in surface dust thickness (shaded) after one year, using the wind stress (top row) and dust devil (bottom row) lifting parameterizations and passive dust transport, for o=25° (experiment presPAS, left column) and 45° (experiment o45PAS, right column). (The middle row shows results using wind stress lifting with active dust transport, experiments presAC and o35AC, discussed in section 4.2.) The amount of wind stress lifting is greatly increased for o=45°, hence contour intervals ten times larger are used to plot both lifting and net accumulation.

An important point is that both lifting rates and deposition rates are needed to determine the net change in surface dust cover. The zero lifting contour does not always coincide with the border between net accumulation and net removal (where blue meets green in these plots), indicating the importance of transport and deposition as well as lifting alone. (The zero lifting contour does not appear on the annual mean dust devil lifting plots, as during the course of a year there is some lifting everywhere using the current parameterization.) Regions in which some dust lifting occurs are often regions of net dust accumulation overall, due to deposition rates exceeding lifting (this occurs over almost all northern high latitudes, for example).

In all simulations the pattern of dust deposition is determined partly by local re-deposition, explaining for example the peak in dust accumulation between two regions of strong wind stress lifting in the Chryse WBC region for o=25°. Also important is fallout of dust which has been carried and mixed within the main atmospheric circulation. At the dustiest periods, around the solstices, atmospheric dust is largely transported across low and midlatitudes within a cross-equatorial Hadley cell. As air columns are forced up over topography the dust within them will concentrate near the surface, increasing deposition rates. Also, in the lower atmosphere dust is transported most rapidly across the equator (from the descending to the rising branch) within the WBC regions, whereas in the intervening regions – primarily the uplands of Tharsis, spanning the equator, and south from Arabia into Noachis – wind velocities are far smaller. Dust thus has more time to fall to lower levels (eventually to the surface) before again being carried aloft. These arguments depend on a relatively uniform distribution of dust within the Hadley cell, however. Thus the strongest correlation between topography and deposition is found when most dust is lifted near the rising Hadley cell branch, allowing time for it to be well mixed before nearing the surface again, and the weakest

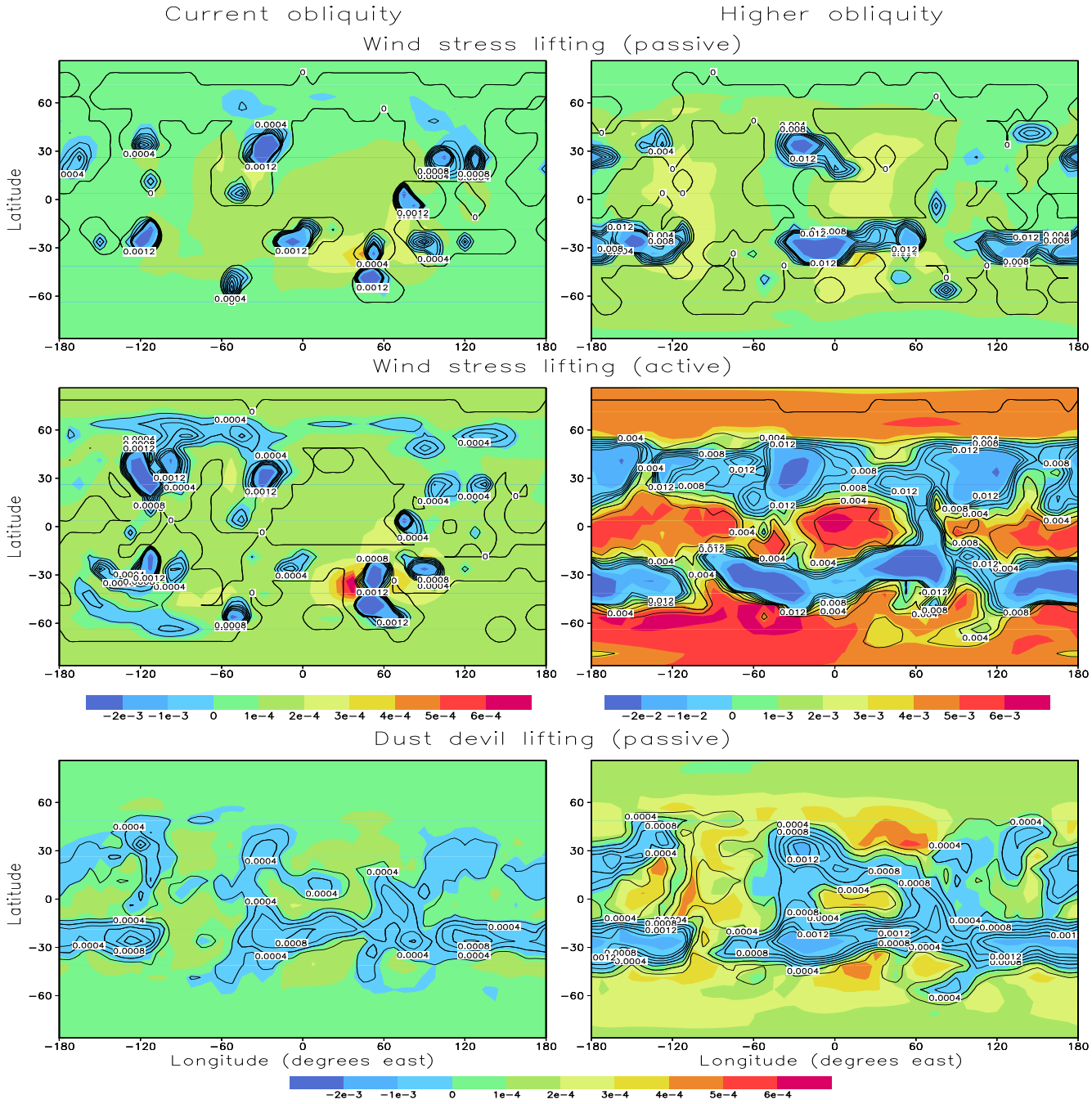

Figure 7: Newman et al. Patterns of wind stress and dust devil lifting and net change in surface dust cover for two obliquities.

correlation is found when strong lifting also occurs near the descending branch. So for example a stronger correlation is produced for passive wind stress lifting (top row of Fig. 7) at 45° (right) than at the current obliquity (left).

The main feature of the passive wind stress lifting results is the strong net removal within the WBCs and, increasingly as obliquity (hence the strength of the mean meridional circulation, and the strength and area of associated summer westerlies) increases, within a zonal collar in southern mid-latitudes. Two regions of net accumulation increasingly dominate, one centred on 30°E and the other on 120°W, both extending between ∼40° north and south of the equator (excluding regions of strong erosion between ∼20° and 35°S). The details of this result are, however, sensitive to the dust loading prescribed in the MGCM. If dust levels are increased in northern winter, for example, this will produce a stronger meridional circulation, resulting in more lifting within the WBC regions and possibly significant lifting in a band of northern mid-latitudes. These affects are discussed further for active dust simulations (which do have higher dust loadings at this time of year) in section 4.

For dust devils the change in surface dust cover for o=45° can be plotted using the same contour intervals as for o=25°, due to the smaller increase in lifting rates as obliquity is increased than for wind stress (as discussed in section 3.2.1). These results suggest that dust devil lifting is probably less important at high obliquities, relative to wind stress lifting, than it is at present. However, the fact that dust devils have little or no link to the varying circulation at different obliquities, but rather to the less radically changing distribution of solar heating, suggests that at low obliquities (when wind stress lifting is greatly reduced) dust devils may be the main source of atmospheric dust.

3.2.3 Comparisons with observed dust deposits

Thermal inertia should be high in regions with little dust and low in regions where a lot of dust is present (e.g. Jakosky et al. 2000), so may be used to assess the current surface dust distribution. Maps of thermal inertia derived from MGS TES spectra are shown in e.g. Mellon et al. (2000) and Ruff and Christensen (2002). Ruff and Christensen (2002) also extract a ‘dust cover index’ based on using both lambert albedo and thermal inertia, though this is more representative of the material lying on the surface than thermal inertia (which probably indicates the proportion of dust within the first few centimeters of the surface), hence there are some differences. Thermal inertia is thus more useful in identifying longer term accumulation and hence thicker dust deposits. Based on the most recent thermal inertia maps, there is a large region of high dust

content over Arabia ($\sim$10°W – 60°E, 10°S – 40°N), and another broad region of high dust content stretching from Elysium through Amazonis and over Tharsis ($\sim$140°– 180°E and 180°– 70°W, covering most latitudes from 15°S – 40°N).

If the observed regions of high dust content formed recently (say in the last 200,000 years, during which time obliquity was close to its present value), and if local dust production (via erosion) is ignored, then such regions should coincide with MGCM predictions of peak dust accumulation for the current obliquity. If, however, the observed regions formed over much longer timescales, or were mostly formed at a time in the past when higher obliquities dominated, they should be a better match to predictions of peak accumulation regions at higher obliquities, when many times more lifting probably occurs, resulting in far greater accumulation rates.

Considering first wind stress dust lifting using passive dust transport (upper row of Fig. 7), peak accumulation occurs in the southern hemisphere for the current obliquity (left plot) and there is no apparent anticorrelation between this plot and maps of thermal inertia. At higher obliquities – at 45° (right plot), and also at 35° (not shown) – there are two other regions of peak accumulation further north, coinciding with the Arabia and Tharsis regions observed to have high dust content. This suggests that the dust observed in these areas may have accumulated over longer timescales, or have mostly taken place more than 500,000 years ago (when Mars last had obliquities of $\sim$35° or greater). Yet for all obliquities the MGCM fails to predict peak accumulation over the Amazonis or Elysium regions observed to have high dust content.

The accumulation rates predicted by the MGCM can be used to provide an estimate of the age of these deposits if their thickness is known. Christensen (1986) estimated the thickness of the low thermal inertia regions to be between 0.1 and 2m, using thermal, radar and visual data. Obliquities have varied between 15° and 35° over the past 4Myrs, being roughly equally split between being greater than or less than 25°. A conservative estimate of the mean accumulation rate during this period is therefore that for 25° (given that accumulation is greatly reduced for low obliquities, but is considerably more than doubled for o=35°), $\sim 1.5\times10^{-4}$cm yr^{-1} in central Arabia. This gives an upper limit on their age as between $\sim$67,000 and 1.3 million years. There is an inconsistency here, noted also by Haberle et al. (2003), in that the results show large parts of these regions to have been accumulating dust for all obliquities (presumably going back many millions of years), but also imply that, if the estimated thicknesses are correct, they can only have begun forming $\sim$1.3Myr in the past. This would suggest either that the net accumulation rates predicted using wind stress lifting and passive dust transport are overestimates of the true values, or that the thicknesses

estimated by Christensen (1986) are much too small.

The above analysis did not consider the effects of dust devil lifting. Looking at the pattern of dust accumulation for dust devils, the net removal in e.g. central Arabia and over much of Tharsis would bring down accumulation rates in these specific regions. Dust removal by dust devils would become less important relative to the effects of wind stress lifting at higher obliquities, which might help to explain the closer similarity between high obliquity accumulation patterns and currently observed surface dust content. But wind stress lifting with active dust transport can also produce erosion over much of the high dust content regions (see section 4.2). Clearly, to model dust accumulation rates correctly both wind stress lifting, dust devil lifting and the effects of radiatively active dust transport should be included.

3.2.4 Net polar dust accummulation and the polar layered terrain

Figure 8 shows the change in thickness of polar dust deposits over one year for four obliquities (experiments o15PAS, presPAS, o35PAS and o45PAS), using passive dust transport and wind stress lifting. Here polar is defined as 75°–90°N and S. The absence of dips in these curves demonstrates the lack of any net removal from polar regions. There are several clear trends – firstly, increased accumulation at both poles as obliquity is increased, due largely to greater atmospheric dust levels overall. Secondly, as obliquity is increased the pole gaining most dust switches from the north to the south. Lastly, as obliquity is increased the relative accumulation during northern summer becomes increasingly important in these passive dust experiments. Unfortunately, due to the complex nature of the results described here, the above trends will not necessarily be valid for all dust scenarios, and when active dust is used only the first is certain to hold for all parameter values.

Relative deposition rates over the north and south poles depend on atmospheric transport as much as on where dust is lifted. Provided there is a moderately strong meridional circulation, polar deposition over the winter pole is generally due more to upper level, cross-equatorial transport of dust lifted in the summer hemisphere than to dust lifting at high winter latitudes. For o=25°, for example, much of the dust deposited over the north pole after $L_s \sim 250°$ was lifted in the 22.5°–45°S range (see Fig. 6) then transported into the winter hemisphere. Only some of this lifted dust reaches higher summer latitudes, to produce a smaller increase in dust thickness over the south pole.

During northern winter for o=45°, however, there is clearly transport over the summer (south) as well as the winter (north) pole, with greater dust accumulation over the south pole despite the cross-equatorial

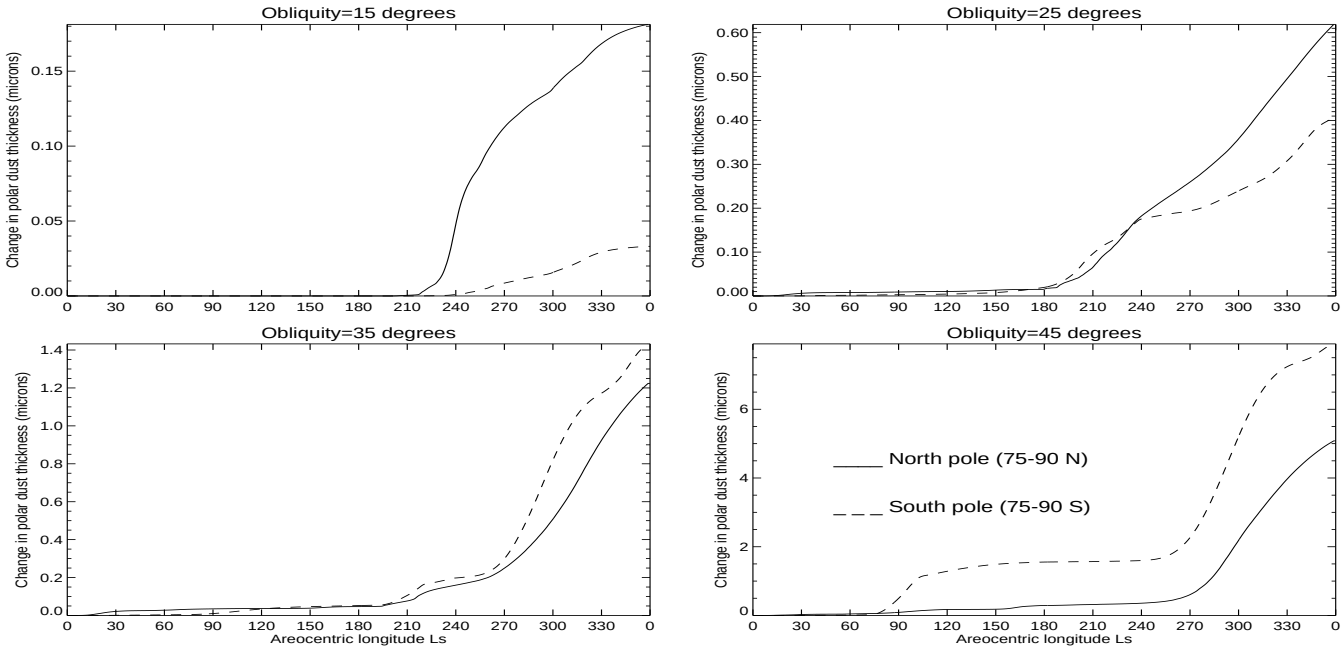

Figure 8: Newman et al. Polar dust accumulation for four obliquities using wind stress lifting.

circulation being stronger than during northern summer. This is due in part to the low level branch of the Hadley cell extending further polewards for higher obliquities. It therefore carries more of the dust raised in southern mid-latitudes further towards the pole, before carrying much of it to higher levels and into the opposite hemisphere. For greater dust opacities a tidally forced cell, which rises in summer mid-latitudes and descends over the summer pole, may also increase poleward dust transport.

Overall, the passive dust transport results suggest that dust deposition over south polar regions is minimal for low obliquities, increasing to extremely large amounts for high obliquities. Over north polar regions, dust deposition is small (though greater than in the south) for low obliquities, increasing to very large amounts (but less than in the south) for high obliquities. How this may impact the formation of of the polar layered terrain would require careful modeling of water ice as well as dust deposition (including dust scavenging during ice formation).

Dust devils (see Fig. 9) show a similar trend of peak accumulation over the north pole at low obliquities, this switching gradually to the south pole as obliquity is increased. The main difference is that polar accumulation rates are actually higher in the north for o=15° than for o=25° (and are comparable in the south). Polar dust thickness also increases more gradually than for wind stress lifting, particularly at low obliquities. These differences are due to the broader spread of locations and times over which dust devil lifting occurs (relative to wind stress lifting), meaning that dust devil lifting is more affected by increases in the area of

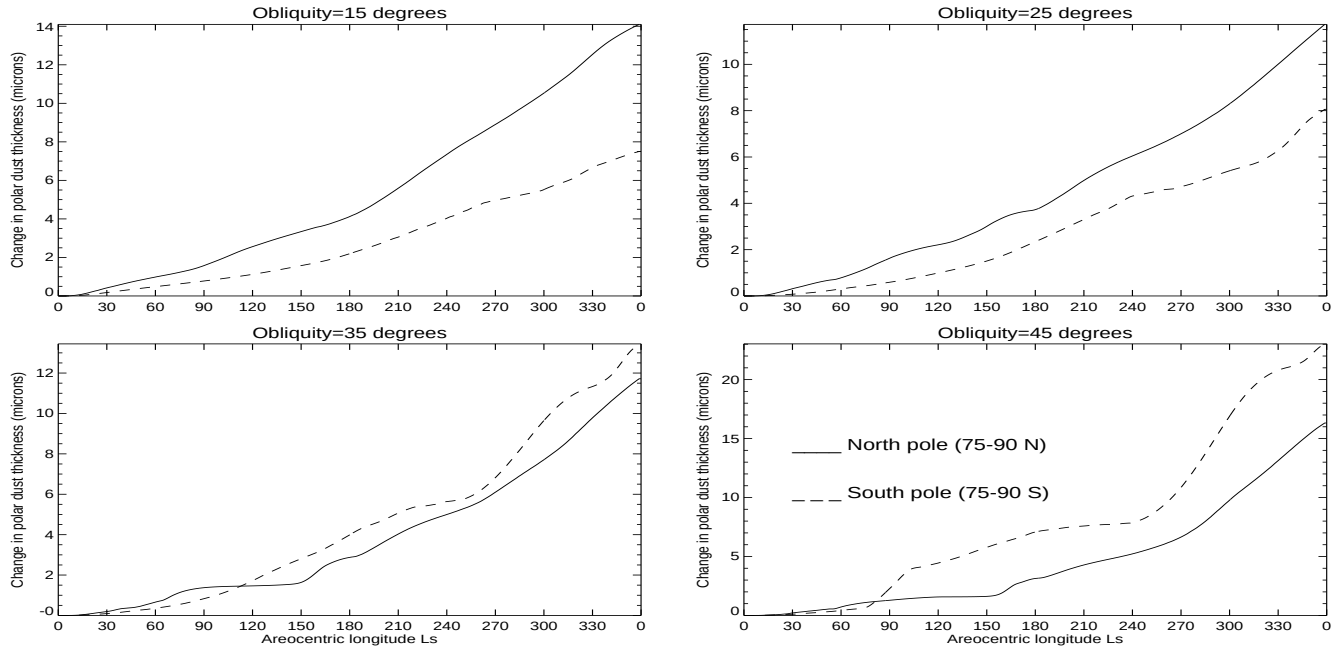

Figure 9: Newman et al. Polar dust accumulation for four obliquities using dust devil lifting.

the winter hemisphere covered by CO_2 ice (which prevents lifting). At o=15° for example, dust devil lifting can continue to ∼55°N throughout the year, whereas at o=25° no lifting occurs north of ∼40°N for almost a third of the year. At higher obliquities, however, increased lifting rates during local summer more than compensate for the loss of ice-free surface in the fall to spring hemisphere, hence accumulation rates at o=35° are higher than those at 25°. These results reinforce the idea that dust devil lifting may become more important to the rearrangement of surface dust at low obliquities.

4 The effect of varying obliquity with radiatively active dust transport

4.1 The atmospheric circulation and dust lifting

The experiments shown previously used a single, prescribed dust distribution, which was not strictly consistent with the circulation produced and the predicted dust lifting. The experiments described here, using parameterized lifting and radiatively active dust transport, allow feedbacks to occur and the dust distribution to evolve consistently, and should therefore better represent the true behavior on Mars. These experiments (presAC and o35AC) include wind stress lifting only (ignoring here the effect of ‘background’ dust devil lifting) with the same lifting parameters and threshold stresses used at both obliquities to produce results which are consistent with each other, as for the passive runs.

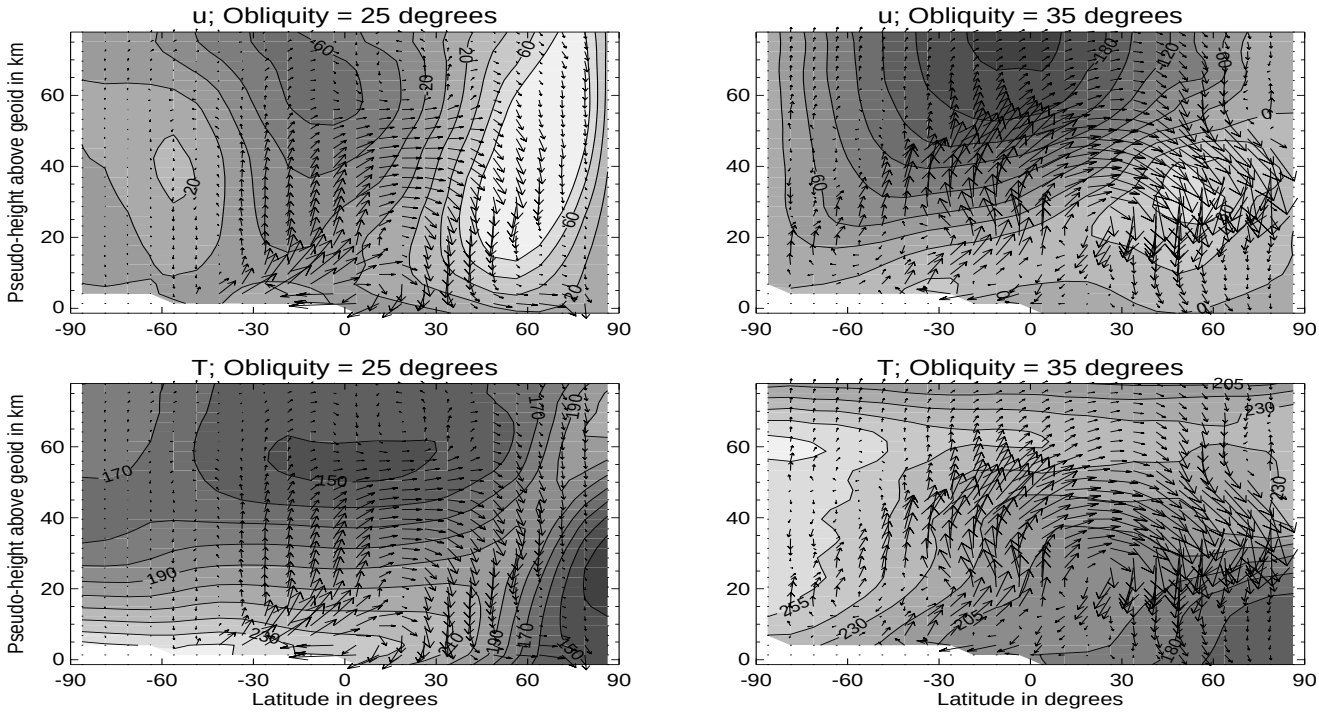

Figure 10: Newman et al. A zonal mean solsticial circulation for o=25° and 35° with active dust.

Results are shown for o=25° and 35° only, because the positive feedbacks produced such high opacities above o=35° that the MGCM's radiative transfer scheme became unstable. As discussed in section 6, however, it is likely that such rapid growth in dust levels would not occur in reality.

The passive dust experiments for different obliquities already differed in terms of the strength of the summer meridional circulation and associated wind stress lifting. The first order effect of including radiatively active dust transport is therefore to enhance these differences due to positive feedbacks between circulation strength and dust lifting. Figure 10 shows an increase in the strength of the northern winter circulation for both obliquities (the passive dust results for o=35° were intermediate between those for o=25° and o=45° shown in Fig. 3) when active dust transport is used. The increase is far greater for o=35°, however, with different contour levels and arrow lengths even being required. And whereas for passive dust the southern summer wind stress lifting peak in the 22.5°– 45°S latitude band was nine times larger for o=35°(not shown) than for o=25°, Fig. 11 shows that it is more than thirty times larger for the active dust case. At o=35° the strong positive feedbacks on lifting during southern summer produce such huge opacities at this time of year that this peak completely dwarfs that during northern summer, which is however still larger than that produced in the passive case.

Second order effects, which include interactions between the atmospheric dust distribution and atmo-

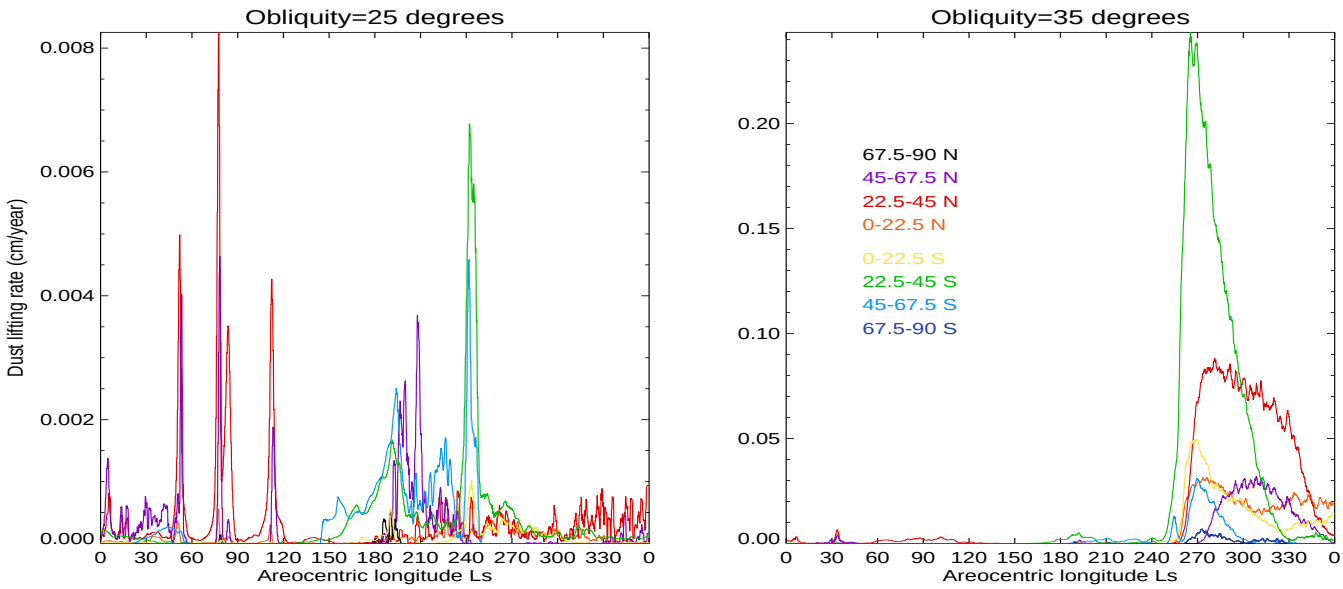

Figure 11: Newman et al. Wind stress dust lifting for o=25° and 35° with active dust.

spheric wave forcing, and the presence of local feedbacks (positive and negative) between dust distribution and flow regimes, are more dependent on the exact details of the wind stress parameterization used. These include, for example, the addition of several strong lifting peaks in the northern hemisphere during summer for the active o=25° case, resulting from strong positive feedbacks on lifting at the edge of localized dust clouds in a relatively clear atmosphere.

A further effect is the smaller seasonal CO_2 ice cap which forms in the northern hemisphere during winter for o=35°, compared to the passive dust result. This may be due to far greater adiabatic warming being caused by stronger downwelling in northern high latitudes (though eddy heat fluxes probably play at least a minor role). This allows dust lifting potentially to extend roughly 15° further to the north compared with the passive simulation which, as discussed below, has strong implications for net surface dust removal. It also affects the dominant wind direction in northern midlatitude regions, which returns to being from the NE during winter (as predicted for the present day) rather than winds from the WSW during summer being expected to dominate as obliquity is increased. Hence there could be a significant impact on the conclusions of section 3.1.3 if such high dust loadings and strong circulations actually occur at high obliquities (see discussion in section 6.1).

4.2 Regions of dust accumulation

The middle row of Fig. 7 shows dust lifting and net accumulation for the active dust experiments presAC (left column) and o35AC (right column). At the surface the far stronger, broader Hadley circulations produced in active dust runs as obliquity is increased produce stronger meridional flows across the equator and extend the strong associated zonal winds to higher latitudes. This has the effect of increasing the amount of net dust removal within the WBC flows, resulting in net erosion in a band stretching north across the equator from Hellas for the o=35° simulation. There is also net erosion over nearly the entire 20°– 45°S latitude band during southern summer (where strong westerlies develop). Erosion also occurs in northern mid-latitudes during northern summer, though it is less significant due to the weaker circulation at this time of year.

There is increased dust removal from high latitudes in both hemispheres for the present day (o=25°) active dust simulation, due to changes in the amount and vertical distribution of dust compared to that which was prescribed in the passive dust case. For example, lower opacities in northern spring result in stronger cap edge flows and increased baroclinic wave activity, as expected (see respectively Siili et al. 1999; Zurek et al. 1992), hence more associated dust lifting.

The more extensive circulations at both obliquities (particularly for o=35°) lead to increased poleward transport of dust. At o=35°, the combination of this with a far dustier atmosphere therefore produces greatly increased polar accumulation rates (both relative to o=25° active results and relative to o=35° results using passive dust transport).

For sufficiently high dust loadings there is substantial net erosion in northern mid-latitudes during southern summer also (as shown in the high obliquity dust lifting plot of Fig. 11). Easterlies form here (via conservation of angular momentum) as the strong return flow of the Hadley cell's lower branch moves equatorward in the northern hemisphere, and produce particularly high near-surface wind stresses due to the higher surface pressure over the lower topography in that hemisphere. These easterlies were present (though weaker) in the passive dust simulation, but there was extensive CO_2 ice cover (to $\sim$30°N at L_s=300°). For the active case, however, the surface is free of ice to $\sim$45°N by this time of year, allowing substantial dust removal from the mid-latitude regions, as shown in the middle right plot of Fig. 7.

5 The effect of varying eccentricity and areocentric longitude of perihelion

5.1 The atmospheric circulation

Obliquity variations change the relative latitudinal distribution of solar insolation away from equinox, and thus have a major effect on polar cap extent and on the peak forcing location of the meridional circulation, both of which strongly affect near-surface winds. Varying Mars's eccentricity or areocentric longitude of perihelion, by contrast, changes the amount by which the response to solar heating at a particular time of year dominates, and the time of year at which this occurs. In general, therefore, the effect on the general circulation and wind stress dust lifting is less significant than the effect due to obliquity variations, although changes to the amount of seasonal ice cover at a given time of year can have a significant impact. The timing of perihelion decreases in importance as eccentricity is decreased (ceasing to matter for a circular orbit). But for moderate to high eccentricities, and with a constant value of obliquity, the atmospheric response is determined by the extent to which l aligns with a solstice or equinox (the former producing stronger circulations than the latter). If l occurs near a solstice, the response will also depend on whether it is northern winter or summer (the former again producing stronger circulations than the latter, due to the effects of the hemispheric dichotomy discussed below).

Figure 12 shows zonally averaged temperatures and zonal winds, and the residual mean circulation, for both solstices for a simulation with e=0, but otherwise with present day orbital settings (experiment e0PAS). The distribution of solar insolation from summer to winter latitudes is therefore the same for both northern and southern summer. For a featureless, smooth planet this would result in almost identical distributions of solar heating (assuming constant or mirror image dust loadings) and mirror image solsticial circulations. This is clearly not the case for Mars, the main feature of Fig. 12 being the asymmetry between the solsticial circulations, with that during northern winter significantly stronger.

Figure 13 shows the same results for simulations in which perihelion occurs in northern summer (l=71°), at exactly the opposite time of year to that at which perihelion presently occurs, but otherwise with present day settings (experiment l71PAS). For a featureless, smooth planet the northern summer (winter) circulation would therefore be expected to be a mirror image of that currently produced during northern winter (summer). Again, this is not the case for Mars, with the circulation at northern winter solstice for l=71° approximately as strong as at northern summer solstice (if not stronger), despite coinciding with aphelion (when roughly a third less solar insolation is received).

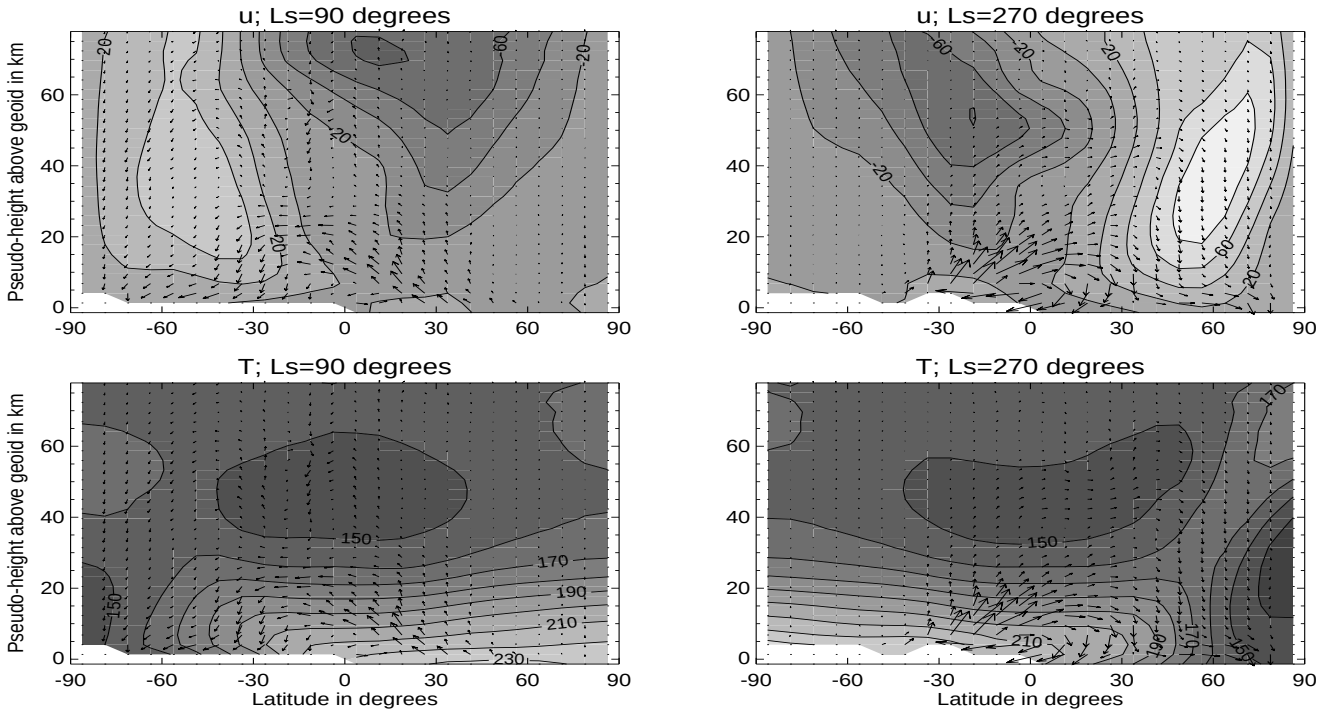

Figure 12: Newman et al. The zonal mean solsticial circulations for e=0.

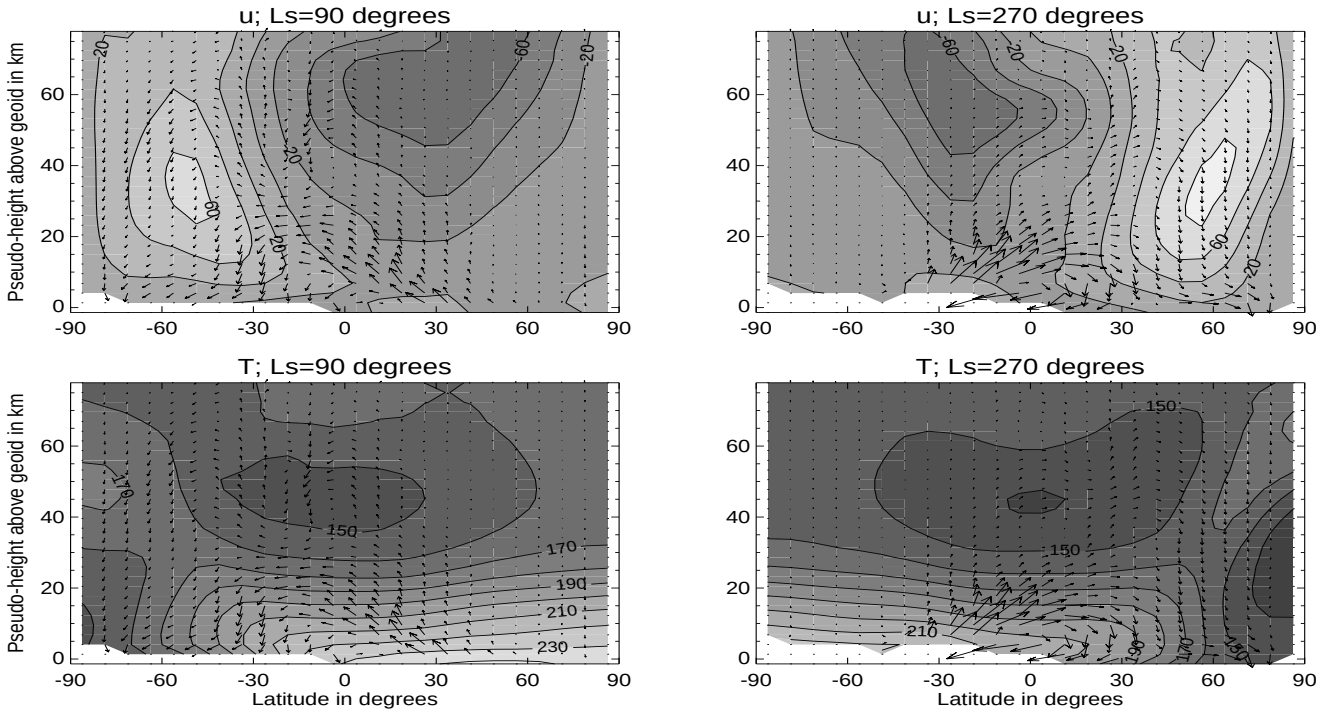

Figure 13: Newman et al. The zonal mean solsticial circulations for l=71°.

The reason for these asymmetric results is that Mars is neither featureless nor smooth, its surface having significant variations of albedo and thermal inertia (affecting the absorption of radiation) and topography (affecting the height above the geoid to which radiation penetrates and at which near-surface air is heated by the ground, and also impeding the flow). These can also act in more subtle ways by changing the wave structure of the atmospheric flow. Joshi et al. (1995) pointed out that the observed asymmetry in Mars's solsticial circulations is not simply due to perihelion occurring during southern summer, and Richardson and Wilson (2002) showed the presence of an annual mean bias by considering the effect of changing perihelion on the simulated annual mean mass streamfunction. They found this to be dominated by the northern winter hemisphere cell for both l=71° and 251°, whereas the southern winter hemisphere cell would have dominated for l=71° if the orbital configuration (and magnitude of solar insolation) were most important. They then showed that this bias was essentially eliminated if the hemispheric dichotomy in topography was removed. Takahashi et al. (2003) have explored this further, and shown a similar dependence on the elevated southern hemisphere using another Mars general circulation model.

Such biases can be most easily investigated for e=0, since for a featureless and smooth planet this situation would produce mirror image circulations at the two solstices as well as a highly symmetric mass streamfunction when averaged over the entire year. Figure 14 shows annual mean mass streamfunctions for e=0 under different conditions: (1) no alterations; (2) topographic dichotomy removed; (3) uniform, smooth surface but with MGS Mars Orbiter Laser Altimeter (MOLA) topography used to model surface and gravity wave drag; and finally, (4) a uniform, smooth surface without drag. The plot for case (4) is, as expected, completely symmetric, since there are no longer any hemispheric asymmetries, yet the case (2) plot is significantly more symmetric than that for case (1), indicating the importance of the hemispheric topographic dichotomy in biasing the mass streamfunction.

If the solsticial circulations are examined for the different cases, removing the dichotomy has a similar effect in reducing the bias in regions where the mass streamfunction has significant amplitude. Figure 15 shows zonal mean temperatures and the residual mean circulation for cases (2) and (4). Comparing these results with those for case (1), shown in Fig. 12, the circulation is far more symmetric between the solstices below $\sim$40km and away from high latitudes once the topographic dichotomy has been removed. Above this and at higher latitudes, however, the circulation is still stronger in northern than in southern winter, with a far greater polar warming over the winter pole. Not until all asymmetries have been removed is the circulation (including near-surface wind patterns) completely symmetric.

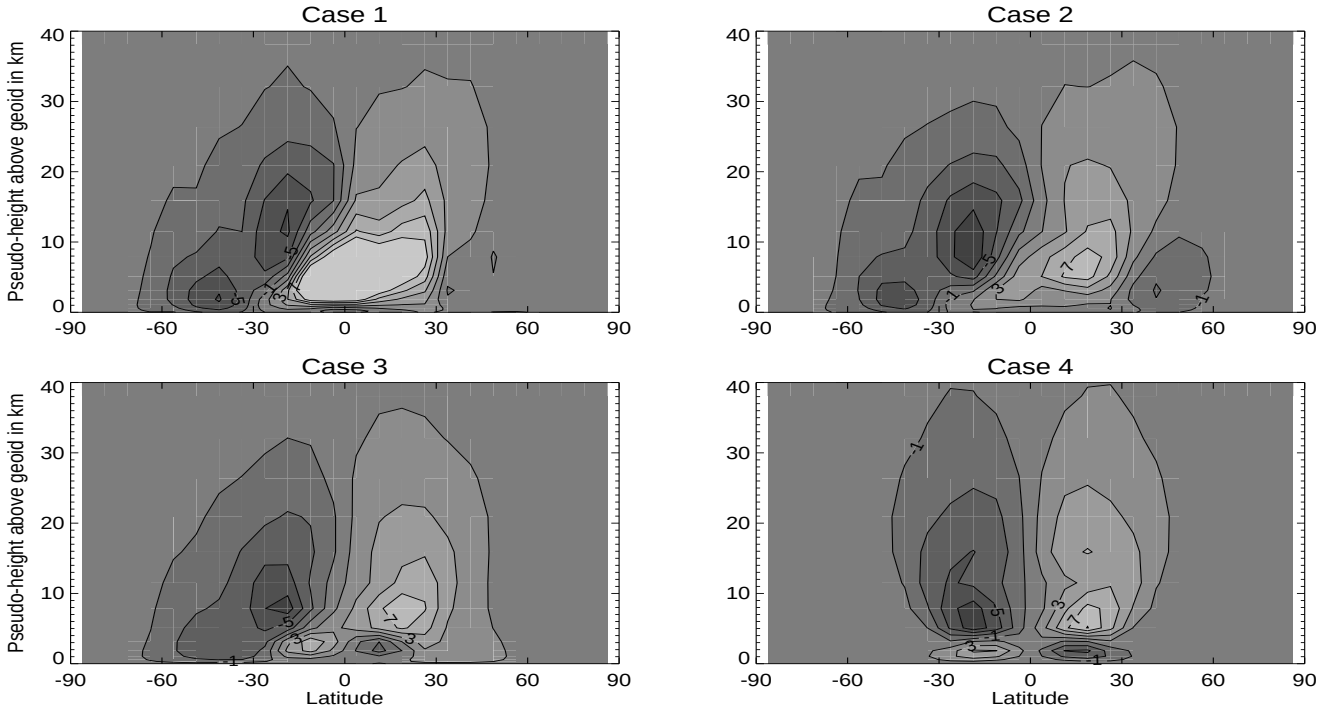

Figure 14: Newman et al. Annual mean mass streamfunctions for four e=0 cases.

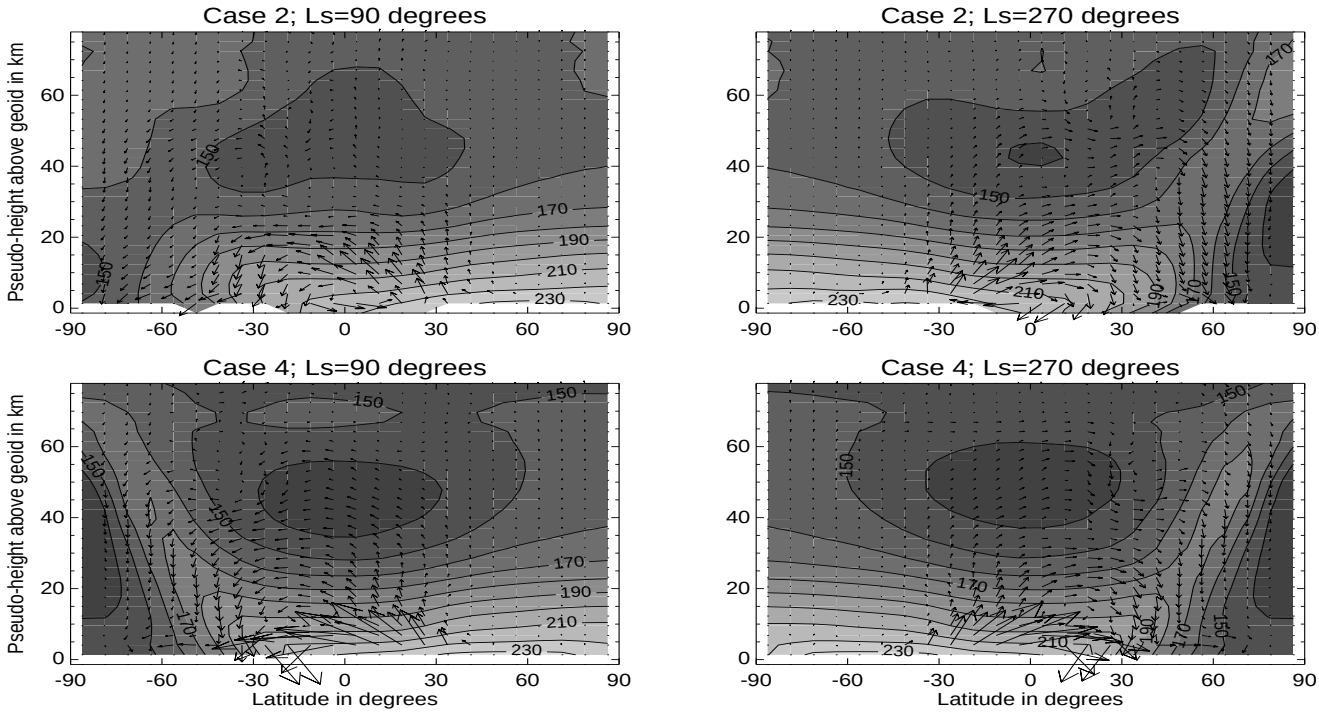

Figure 15: Newman et al. Zonal mean temperatures and residual mean circulations at solstice for two e=0 simulations.

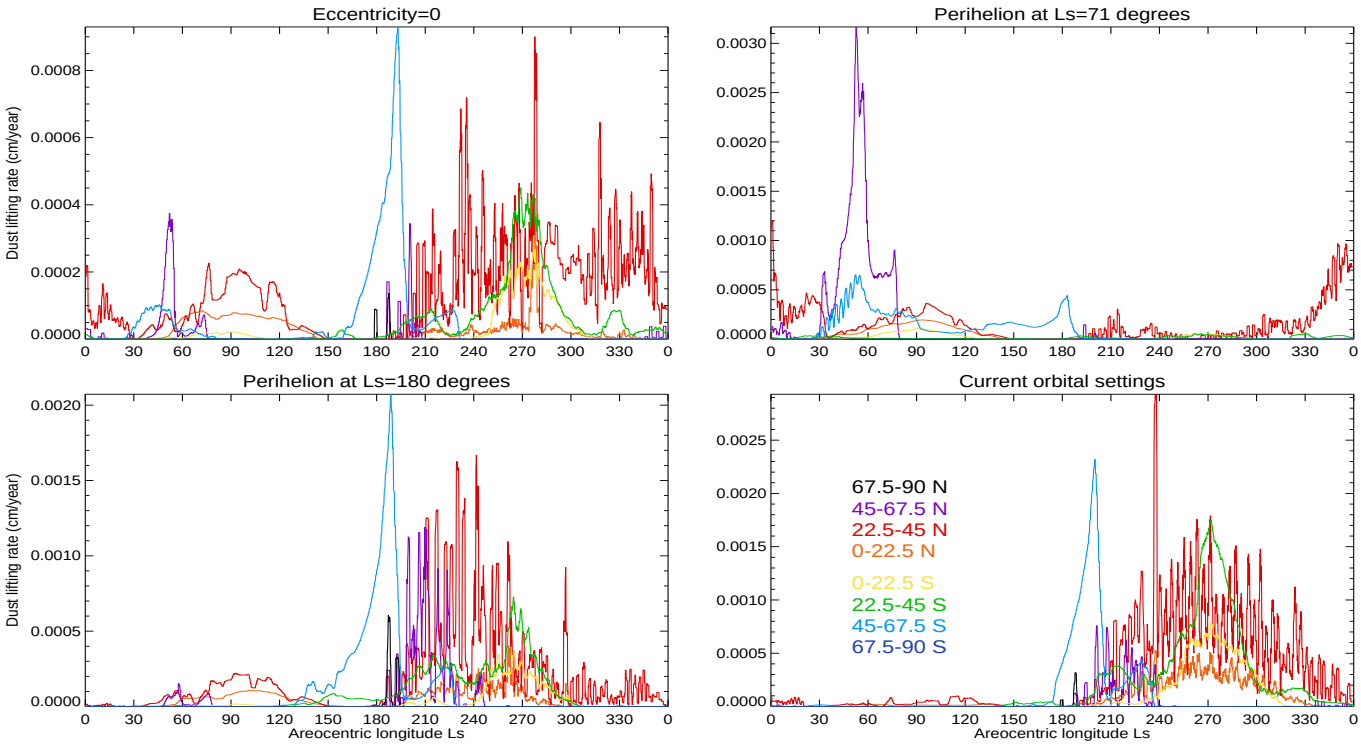

Figure 16: Newman et al. Wind stress dust lifting for two eccentricities and two longitudes of perihelion.

5.2 Dust transport

Figure 16 shows the pattern of wind stress dust lifting in different latitude bands for the e=0, l=71° and l=180° passive dust transport simulations, with results for current orbital settings shown again for comparison. The pattern of dust lifting for e=0, with far more lifting after $L_s \sim 180°$ than earlier in the year, is (apart from having more lifting peaks during northern summer) very similar to that for the present day. This demonstrates clearly that asymmetry between southern and northern summer solstice still exists in the absence of a time of peak solar insolation. Results for l=180° are similar, with northern winter again dominant in terms of lifting. By contrast, the results for l=71° do show a significant switch from southern to northern summer dominance, far more so than might have been anticipated by the change in circulation strength. This is almost entirely due to the larger seasonal north polar cap only having receded to ∼60°N by late spring ($L_s \sim 50°$), resulting in strong off-cap flows and large amounts of lifting at its edge.

Figure 17 shows the change in polar dust thickness with time for one year of the e=0, l=71° and l=180° simulations, again with results also shown for the current settings. For l=71° the north pole receives more dust than the south during northern summer. The circulation is weak compared to the southern summer circulation for l=251°, thus this is due to a combination of reduced cross-equatorial transport by the Hadley

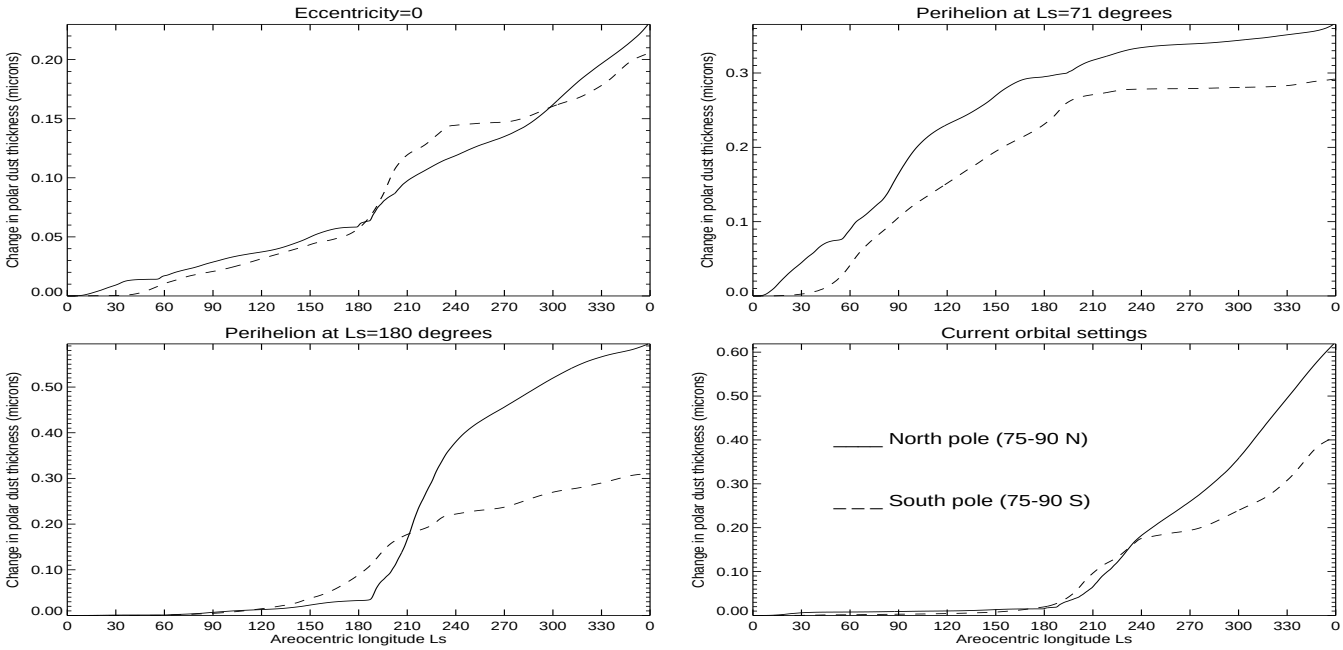

Figure 17: Newman et al. Polar dust accumulation for two eccentricities and two longitudes of perihelion.

cell's upper branch and increased dust lifting at fairly high northern latitudes.

In all cases the amount accumulated at both poles at any time tends to be increased close to perihelion and decreased close to aphelion, though in the absence of these (e=0) there is greater accumulation during northern winter, with results for the other cases showing a northern winter bias also. Overall, accumulation rates are higher as perihelion nears northern winter solstice (since overall this produces the strongest circulations and lifting rates), and are lowest when solar insolation is spread evenly through the year (for e=0). There is also more accumulation over the north pole than the south for the three cases shown (suggesting that north polar accumulation probably dominates for all orbital configurations having $o \leq 25°$).

6 Conclusions

6.1 Changes to the atmospheric circulation due to changing orbital parameters

The MGCM predicts that as Mars's orbital parameters vary with time, the greatest changes to atmospheric circulation and dust transport are due to variations in obliquity. Increasing obliquity affects the relative latitudinal distribution of solar insolation (away from equinox), which has a major effect on polar cap extent and on the peak forcing location of the meridional circulation near solstice. The seasonal CO_2 cap extends over more of the winter hemisphere, and the peak in time-averaged solar forcing occurs at higher

latitudes producing broader and stronger meridional (Hadley) circulations.

At low obliquities permanent CO_2 ice caps form at both poles, significantly reducing mean surface pressures (to $\sim$40Pa for o=5°, and $\sim$350Pa for o=15°), hence also lowering near-surface densities and thus wind stresses.

When active dust transport is included, a wind stress lifting parameter selected to produce realistic results for the current obliquity produces huge amounts of lifting for even o=35°, due to the strong positive feedbacks between atmospheric dust loading, the atmospheric circulation and wind stress lifting. Simulations for o=45° rapidly become unstable (see comments below). In addition, the stronger circulations produced in a dustier atmosphere lead to increased downwelling and adiabatic warming at winter high latitudes, resulting in smaller seasonal caps than in passive runs which in turn affects the surface wind distribution and dust lifting.

The primary effect of varying eccentricity is to change the impact of varying the areocentric longitude of perihelion, which determines when the solar forcing is strongest. The atmospheric circulation is strongest when l aligns with solstice, and there is also a bias from the Martian topography, resulting in the strongest circulations for high e when l is in northern winter.

Near-surface winds associated with a solsticial Hadley circulation (e.g. cross equatorial WBCs and summer midlatitude westerlies) increase in strength as this circulation intensifies at higher obliquities, increasingly dominating over baroclinic, thermal contrast (e.g. cap edge) and topographic flows. Along with changes in the position of the cap edge, these effects produce significant changes in surface wind directions as well as magnitudes.

For passive dust transport the MGCM predicts that at higher obliquities the dominant northern midlatitude ($\sim$25°– 50°N) winds should be from the SW during summer (rather than from the NE during winter, as at present). This is due to the presence of a stronger, broader Hadley cell (and its associated surface winds) during summer, and increased ice cover (reducing near-surface temperature gradients, hence lowering wind magnitudes, far from the cap edge) during winter, as obliquity is increased. If active dust transport is included, however, the MGCM predicts a smaller seasonal ice cap than in the passive run, hence the dominant winds are once again from the NE during winter, implying that care is required in interpreting such results.

6.2 Changes to dust lifting and deposition due to changing orbital parameters

As obliquity increases, for wind stress lifting, the stronger westerlies produced in summer midlatitudes increase dust lifting within bands centred on $\sim$30° latitude (though these move slightly poleward with obliquity, particularly for o=45°). Lifting peaks at the poleward edge of WBC regions, with smaller peaks in equatorial regions within the WBC flows.

There is a smaller change in both the magnitude and pattern of dust devil lifting as obliquity increases. Lifting peaks at $\sim$25° latitude in local summer for all obliquities, the latitude at which atmospheric temperatures lag surface temperatures most strongly in all cases. Peak lifting rates increase more gradually with obliquity than for wind stress lifting, being less tied to the rapidly increasing meridional circulation.

For active dust transport, at o=35° lifting occurs across broader midlatitude regions due to the strong winds associated with stronger, broader meridional circulations in the dustier atmosphere produced. Lifting from northern midlatitudes in winter is enhanced if a smaller seasonal cap forms, though the latter depends on how realistic the high obliquity active dust simulations are in terms of the peak opacities and circulations produced. Care must be taken in interpreting these results as a true representation of what would occur at higher obliquities, and the changes in circulation strength and extent of dust removal shown in Figs. 10 and 11 respectively should be taken as an extreme limit on what might actually occur.

In all cases, the pattern of dust deposition is determined partly by local re-deposition and partly by the fallout of dust which has been carried and mixed within the main atmospheric circulation. There is slight preferential deposition over high topography within the Hadley cell's extent. The effect is strongest when lifting peaks near the rising Hadley cell branch, as this results in the dust distribution being relatively uniform by the time it nears the surface again. Dust lifted near the descending branch, however, will tend to be redeposited before entering the main circulation, and at longitudes similar to those where lifting occurred (which generally peak in the WBC regions which are between topographic highs), thus compensating for the former effect.

6.3 Changes to dust accumulation due to changing orbital parameters

The inclusion of a dust transport scheme within the MGCM is necessary to enable radiatively active dust transport experiments, of key importance in representing real Mars, given the strong feedbacks on dust lifting. But it is also crucial for this study because it allows the MGCM to a) predict dust deposition and net accumulation, as well as dust lifting, and b) constrain lifting parameters by comparing the simulated

atmospheric dust distribution with that observed. Together, (a) and (b) then allow quantitative comparisons to be made between predicted and observed surface dust deposits.

Results show that the boundary between net erosion and net accumulation does not necessarily coincide exactly with the zero lifting contour, and more importantly, that the amount of accumulation varies considerably even within regions where only deposition occurs.

6.3.1 Potential long term dust deposits

As obliquity increases, regions of peak net dust accumulation north of $\sim$30°S are increasingly restricted to Arabia and Tharsis, in agreement with observations of peak dust content here, though Amazonis and regions around Elysium are less apparent in simulations than in observations.

For active dust transport, the scouring of dust from northern as well as southern midlatitudes at higher obliquities limits the areas with peak accumulation to $\pm$15° of the equator, though the longitudinal match to observations is improved. There is significant accumulation in Arabia and from Elysium, over Amazonis through to Tharsis, with net erosion clearly peaking within the WBCs. Erosion over the Tharsis peaks is reduced because of smaller slope winds in the dustier atmosphere. Accumulation south of the strong southern hemisphere erosional band is due to enhanced polewards transport of dust raised in the south during summer.

The MGCM predicts current accumulation rates of $\sim 1.5 \times 10^{-4}$ cm/year in the Arabia region. The estimated thickness of dust deposits here (Christensen 1986) then suggests that they were formed in $\sim$67,000–1.3 million years, though this timescale is inconsistent with the results shown here, since the MGCM predicts that a large part of this region will accumulate dust over a range of orbital conditions. The greater correlation between higher obliquity results and observations of dust content might suggest that they formed mostly under higher obliquity conditions, but in this case the accumulation rates would have been even higher.

A small amount of lifting from these regions would result in lower net accumulation rates. Unfortunately, lifting predicted here in both dust devil and active wind stress experiments does not produce this result, instead scouring the northern half of dust and (in the case of active lifting) increasing net accumulation in the equatorial areas and to the south. It is possible that the estimated dust thicknesses are too small, or that a more complex model is required, with combined wind stress and dust devil lifting, and active transport. A full representation would also include a limited surface dust supply and ice scavenging, both of which may limit the strength of the storms and hence circulations produced, strongly affecting lifting in northern midlatitudes.

In summary, for high obliquities with wind stress lifting only, the MGCM predicts peak net dust accumulation over the Tharsis and Arabia low thermal inertia regions. For stronger circulations (produced in an active dust simulation) the MGCM predicts peak accumulation over the equatorial portions of these regions and also in the low thermal inertia regions of Elysium and Amazonis. If there is no surface ice cover in northern mid-latitudes in winter for the latter case, or if dust devil lifting is included, there is net removal from the more northerly portions of the low thermal inertia regions. This suggests that only the equatorial low thermal inertia regions are dust sinks for all orbital settings, and thus that they may have the highest dust content.

6.3.2 Polar accumulation rates

Dust devil and wind stress lifting is negligible over polar regions (defined as 75°– 90°) for all orbital configurations shown, thus net accumulation here is solely due to deposition. As obliquity increases, polar accumulation rates increase for wind stress lifting due to the higher dust loadings overall, and the stronger, broader transport circulations (particularly for active dust) which carry more dust to the poles. The largest accumulation rates occur when perihelion coincides with southern summer, and peak for high values of eccentricity (giving the strongest solar forcing at perihelion), with weaker rates as perihelion nears an equinox.

For dust devil lifting, polar accumulation rates also increase with obliquity above o=25°, though less rapidly as lifting (hence the dust load produced) is only slightly linked to the stronger surface winds. In active dust simulations the negative feedbacks on dust devil lifting would further reduce this. Polar accumulation rates are higher at o=15° than at o=25°, due to the reduction in surface ice cover at the lower obliquity, which is significant for dust devil lifting as it is more widespread both spatially and temporally. Thus polar dust accumulation at low obliquities may be increasingly due to dust lifted by dust devils.

For all cases discussed, the pole receiving most dust shifts from north to south as obliquity is increased. For low obliquities much of the dust raised in the summer hemisphere is transported across the equator without nearing the summer pole, hence peak lifting in southern summer midlatitudes produces more accumulation at the north pole. At high obliquities, however, the meridional circulation extends closer to the pole in both hemispheres, hence more of the dust raised in the south in summer reaches high southern latitudes before being carried north, raising south polar accumulation rates.

6.4 Future work

The strength of positive feedbacks on wind stress dust lifting, particularly in high obliquity simulations, is a major concern which must be addressed before work can progress. One effect absent from the MGCM which would affect this is the process of dust scavenging by ice particles during nucleation. This will become increasingly important at higher obliquities, when warmer poles result in greatly increased atmospheric humidity and cloud water ice (e.g. Jakosky et al. 1995; Mischna et al. 2003). A further effect of increased water vapor abundances is the effect on surface water ice (rather than CO_2 ice) cover, which may have a huge impact if it prevents dust lifting in for example the northern mid-latitude regions activated during a global dust storm. Mischna et al. (2003) predict water ice cover over most of the northern hemisphere in winter for obliquities 35° and higher. Thus even if temperatures were raised sufficiently to prevent such a large CO_2 ice cap forming, they would also need to be high enough, given the high partial pressures of water vapor at this time, to prevent a large water ice cap forming, which could itself prevent the northern dust lifting. Scavenging is also of major importance in predicting polar dust and ice accumulation rates for comparison with observations of the polar layered terrain, and would require the inclusion of a water transport scheme (currently being validated within the MGCM, Böttger et al. 2004) as well as a microphysics scheme to couple the two properly. Another effect not examined here is the use of a finite dust supply on the Martian surface, such that some regions can be entirely depleted of dust during a simulation. In preliminary MGCM experiments this has been found to increase the amount of interannual variability, by continuously resetting the surface boundary condition for dust lifting. These effects must be explored, and their impact assessed, before the results such as those shown in section 4 can be judged to be realistic.

Acknowledgments.

We gratefully acknowledge support for this work from the UK Particle Physics and Astronomy Research Council, and thank our reviewers for their suggestions and constructive criticism.

References.

Andrews, D. G., Holton, J. R., Leovy, C. B., 1987. Middle Atmosphere Dynamics, Academic Press, Orlando, Florida.

Basu, S., Richardson, M. I., Wilson, R. J., 2004. Simulation of the Martian dust cycle with the GFDL Mars GCM. J. Geophys. Res. (submitted).

Böttger, H. M., Lewis, S. R., Read, P. L., Forget, F., 2004. The effect of a global dust storm on simulations

of the Martian water cycle. Geophys. Res. Lett. (submitted).

Bridges, N. T., Greeley, R., Haldemann, A. F. C., Herkenhoff, K. E., Kraft, M., Parker, T. J., 1999. Ventifacts at the Pathfinder landing site. J. Geophys. Res. 104, 8,595–8,615.

Cantor, B., James, P. B., Caplinger, M., Wolff, M. J., 2001. Martian dust storms: 1999 Mars Orbiter Camera observations. J. Geophys. Res. 106, 23653–23687.

Christensen, P. R., 1986. Regional dust deposits on Mars: physical properties, age, and history. J. Geophys. Res. 91, 3,533–3,545.

Clancy, R. T., Sandor, B. J., Wolff, M. J., Christensen, P. R., Smith, M. D., Pearl, J. C., Conrath, B. J., Wilson, R. J., 2000. An intercomparison of ground-based millimeter, MGS TES, and Viking atmospheric temperature measurements: Seasonal and interannual variability of temperatures and dust loading in the global Mars atmosphere. J. Geophys. Res. 105, 9553–9571.

Edgett, K. S., Malin, M. C., 2000. Martian dust raising and surface albedo controls: Thin, dark (and sometimes bright) streaks and dust devils in MGS MOC high resolution images. Conference paper Lunar and Planetary Science, XXXI.

Fanale, F. P., Salvail, J. R., 1994. Quasi-periodic atmosphere-regolith-cap CO_2 redistribution in the Martian past. Icarus 111, 305–316.

Fanale, F. P., Salvail, J. R., Banerdt, W. B., Saunders, R. S., 1982. Mars – The regolith-atmosphere-cap system and climate change. Icarus 50, 381–407.

Fenton, L. K., Richardson, M. I., 2001. Martian surface winds: Insensitivity to orbital changes and implications for aeolian processes. J. Geophys. Res. 106, 32,885–32,902.

Ferri, F., Smith, P. H., Lemmon, M., Rennó, N. O., 2003. Dust devils as observed by Mars Pathfinder. J. Geophys. Res. 108 (E12), doi:10.1029/2000JE001421.

Forget, F., Hourdin, F., Fournier, F., Hourdin, C., Talagrand, O., Collins, M., Lewis, S. R., Read, P. L., Huot, J.-P., 1999. Improved general circulation models of the Martian atmosphere from the surface to above 80 km. J. Geophys. Res. 104, 24,155–24,175.

Greeley, R., Kraft, M. D., Sullivan, R., Wilson, G., Bridges, N., Herkenhoff, K., Kuzmin, R. O., Malin, M., Ward, W., 1999. Aeolian features and processes at the Mars Pathfinder landing site. J. Geophys. Res. 104, 8,573–8,584.

Greeley, R., Kraft, M. D., Kuzmin, R. O., Bridges, N. T., 2000. Mars Pathfinder landing site: Evidence for a change in wind regime from lander and orbiter data. J. Geophys. Res. 105, 1,829–1,840.

Greeley, R., Bridges, N. T., Kuzmin, R. O., Laity, J. E., 2002. Terrestrial analogs to wind-related features at the Viking and Pathfinder landing sites on Mars. J. Geophys. Res. 107, art. no. 5005.

Haberle, R. M., Leovy, C., Pollack, J. B., 1982. Some effects of global dust storms on the atmospheric circulation of Mars. Icarus 50, 322–367.

Haberle, R. M., Murphy, J. R. Schaeffer, J., 2003. Orbital change experiments with a Mars general circulation model. Icarus 161, 66–89.

Jakosky, B. M., Henderson, B. G., Mellon, M. T., 1995. Chaotic obliquity and the nature of the Martian climate. J. Geophys. Res. 100 E1, 1579–1584.

Jakosky, B. M., Mellon, M. T., Kieffer, H. H., Christensen, P. R., Varnes, E. S., Lee, S. W., 2000. The thermal inertia of Mars from the Mars Global Surveyor Thermal Emission Spectrometer. J. Geophys. Res. 105 E4, 9,643–9,652.

Joshi, M. M., Lewis, S. R., Read, P. L., Catling, D. C., 1995. Western boundary currents in the Martian atmosphere: Numerical simulations and observational evidence. J. Geophys. Res. 100, 5,485–5,500.

Laskar J., Levrard, B., Mustard, J. F., 2002. Orbital forcing of the martian polar layered deposit. Nature 419, 375–377.

Lewis, S. R., Collins, M., Read, P. L., Forget, F., Hourdin, F., Fournier, F., Hourdin, C., Talagrand, O., Huot, J.-P., 1999. A climate database for Mars. J. Geophys. Res. 104, 24,177–24,194.

Liu, J. J., Richardson, M. I., Wilson, R. J., 2003. An assessment of the global, seasonal, and interannual spacecraft record of Martian climate in the thermal infrared. J. Geophys. Res. 108 (E8), doi:10.1029/2002JE001921.

Mellon, M. T., Jakosky, B. M., Kieffer, H. H., Christensen, P. R., 2000. High-resolution thermal inertia mapping from the Mars Global Surveyor Thermal Emission Spectrometer. Icarus 148, 437–455.

Mischna, M. A., Richardson, M. I., Wilson, R. J., McCleese, D. J., 2003. On the orbital forcing of Martian water and CO_2 cycles: A general circulation model study with simplified volatile schemes. J. Geophys. Res. 108 (E6), doi:10.1029/2003JE002051.

Murphy, J. R., Pollack, J. B., Haberle, R. M. Leovy, C. B., Toon, O. B. Schaeffer, J., 1995. 3-dimensional numerical simulation of Martian global dust storms. J. Geophys. Res. 100 (E12), 26,357–26,376.

Newman, C. E., Lewis, S. R., Read, P. L., Forget, F., 2002a. Modeling the dust cycle in a Mars general circulation model. 1: Representations of dust transport processes. J. Geophys. Res. 107 (E12), doi:10.1029/2002JE001910.

Newman, C. E., Lewis, S. R., Read, P. L., Forget, F., 2002b. Modeling the dust cycle in a Mars general circulation model. 2: Multi-annual radiatively active dust transport simulations. J. Geophys. Res. 107 (E12), doi:10.1029/2002JE001920.

Pollack, J. B., Toon, O. B., 1982. Quasi-periodic climate changes on Mars – a review. Icarus 50, 259–287.

Rennó, N. O., Burkett, M. L., Larkin, M. P., 1998. A simple thermodynamical theory for Dust Devils. J. Atmos. Sci. 55, 3,244–3,252.

Richardson, M. I., Wilson, R. J., 2002. A topographically forced asymmetry in the Martian circulation and climate. Nature. 416,298–300.

Ruff, S. W., Christensen, P. R., 2002. Bright and dark regions on Mars: Particle size and mineralogical characteristics based on Thermal Emission Spectrometer data. J. Geophys. Res. 107 (E12), doi:10.1029/2001JE001580.

Siili, T., Haberle, R. M., Murphy, J. R., Savijärvi, H., 1999. Modelling of the combined late-winter ice cap edge and slope winds in Mars' Hellas and Argyre regions. Plan. Space Sci. 47, 951–970.

Smith, M. D., 2004. Interannual variability in TES atmospheric observations of Mars during 1999–2003. Icarus 167, 148–165.

Smith, M. D., Pearl, J. C., Conrath, B. J., Christensen, P. R., 2001. Thermal Emission Spectrometer results: Atmospheric thermal structure and aerosol distribution. J. Geophys. Res. 106 (E10), 23,929-23,946.

Takahashi, Y. O., Fujiwara, H., Fukunishi, H., Odaka, M., Hayashi, Y. Y., Watanabe, S., 2003. Topographically induced north-south asymmetry of the meridional circulation in the Martian atmosphere. J. Geophys. Res. 108 (E3), doi:10.1029/2001JE001638.

Toon, O. B., Pollack, J. B., Ward, W., Burns, J. A., Bilski, K., 1980. The astronomical theory of climatic change on Mars. Icarus 44, 552–607.

Touma, J., Wisdom, J., 1993. The chaotic obliquity of Mars. Science 259, 1,294–1,297.

Ward, W. R., 1992. Long-term orbital and spin dynamics of Mars. In: Kieffer, H. H., Jakosky, B. M., Snyder, C. W., Matthews, M. S. (Eds.). Mars, The University of Arizona Press, Tucson, chap. 9, pp. 298–320.

Zurek, R. W., Barnes, J. R., Haberle, R. M., Pollack, J. B., Tillman, J. E., Leovy, C. B., 1992. Dynamics of the atmosphere of Mars. In: Kieffer, H. H., Jakosky, B. M., Snyder, C. W., Matthews, M. S. (Eds.). Mars, The University of Arizona Press, Tucson, chap. 26, pp. 835–933.